2011-01-01

Raman Microscopy: Complement or Competitor

Hugh Byrne
Technological University Dublin, hugh.byrne@tudublin.ie

Ganesh Sockalingum

Nick Stone

Recommended Citation

Byrne, H., Sockalingum, G. &Stone, N. (2011) Raman Spectroscopy: Complement or Competitor?In Moss, D. (ed.) *Biomedical Applications of Synchrotron Infrared Microspectroscopy.* Royal Society of Chemistry, RCS Analytical Spectroscopy Monographs, no.11, pp.105-142. doi:10.1039/9781849731997-00105

CHAPTER 4

Raman Microscopy: Complement or Competitor?

HUGH J. BYRNE,[a] GANESH D. SOCKALINGUM[b] AND NICK STONE[c]

[a] Focas Institute, Dublin Institute of Technology, Kevin Street, Dublin 8, Ireland; [b] Unite MeDIAN, CNRS UMR6237-MEDyC, UFR Pharmacie, Université de Reims, 51 rue Cognacq-Jay, 51096 Reims Cedex, France; [c] Biophotonics Research Group, Gloucestershire Royal Hospital, Great Western Road, Gloucester GL1 3NN, UK

4.1 Introduction

The objective of this chapter is to provide an introduction to Raman spectroscopic microscopy and its potential for biochemical analysis and clinical diagnostic applications, such that it can be compared and contrasted to the techniques of synchrotron and bench-top mid-FTIR spectroscopy discussed elsewhere in this book. Raman spectroscopy is a complementary technique to mid-IR absorption spectroscopy with established capabilities for materials and process analysis. As a bioanalytical and diagnostic technique, similar to FTIR spectroscopy, its potential has been demonstrated although there are many differing technical considerations to be addressed. Raman has potentially significant advantages as well as drawbacks compared to FTIR techniques. Here we endeavour to outline these benefits and pitfalls and project the complementary and competitive usage of Raman techniques.

RSC Analytical Spectroscopy Monographs No. 11
Biomedical Applications of Synchrotron Infrared Microspectroscopy
Edited by David Moss

Published by the Royal Society of Chemistry, www.rsc.org

4.2 Raman Spectroscopy – a Brief History

The Raman effect was proposed and demonstrated by Sir C. V. Raman in 1928,[1] and independently by G. Landsberg and L. Mandelstam.[2] Inspired by the accepted inelastic scattering of X-rays, Raman proposed a ''new type of secondary radiation'' or ''modified'' scattering which resulted from the effect of the fluctuations from the normal state of atoms and molecules associated with vibrations. He demonstrated that in addition to elastic (Rayleigh or Mie) scattering in which radiation scattered by a material has the same energy (frequency/wavelength), light can be inelastically scattered through a gain or loss of photon energy to the molecular vibrations of the material. The spectrum of the inelastically scattered radiation represented a fingerprint of the molecular vibrations within a material. The observation of the Raman effect gave rise to the field of Raman spectroscopy, a versatile alternative to IR (IR) absorption spectroscopy and now a common analytic laboratory tool. C. V. Raman was awarded the Nobel Prize in physics in 1930 for his work, and in 1998 the Raman effect was designated an ACS National Historic Chemical Landmark in recognition of its importance in materials and process analysis.

The Raman effect is extremely weak, and the evolution from its discovery to a laboratory technique is principally one of technological development. In their original work, Raman and Krishnan used sunlight and narrow band optical filters. Mercury arc discharge lamps subsequently became the source of choice, the scattered radiation being recorded on photographic plates. The use of spectroscopic detection followed, but Raman spectroscopy remained largely a curiosity until the advent of the laser in the 1960s, providing monochromatic sources of significant brightness and intensity and variable wavelength such that the intrinsic limitation of the low efficiency of the scattering process could be overcome. Apart from being a weak process, Raman spectroscopy in the ultraviolet (UV)–visible regions suffered greatly from sample fluorescence, scattering and photodegradation, which made the technique less attractive for coloured samples. Nevertheless, Raman spectroscopy became a very popular research tool, for example in the analysis of phonons, electrons, and electron–phonon interaction in high T_c superconductors.[3] In the mid 1980s Raman went through a renaissance with FT-Raman set-ups that operated with near- IRIR lasers such as Nd^{3+}:YAG emitting at 1064 nm, and detection was done via In:Ga:As detectors. This system benefited from the same advantages as Fourier transform IR spectroscopy, viz. high throughput and multiplex advantages and high precision in the frequency scale. Some FT-instruments were built to accommodate both IR and Raman systems using the same interferometer. In the case of FT-Raman, the scattering sample acts as a polychromatic source. By exciting at high wavelength, both sample fluorescence and degradation could be circumvented but at the expense of a lower scattering process. The low sensitivity of the FT-Raman systems was a drawback for biological samples. Dispersive Raman came back into play with the revolution in charged coupled detector (CCD) arrays in the 1980s and 1990s, which added to the benefits of

high laser source intensities. In addition to this, the development of narrow band laser line rejection filters meant that the huge losses in signal from traditional triple monochromator systems could be overcome with the combination of a filter set and a single spectroscopic grating. Furthermore, the significant reductions in acquisition time with multichannel signal detection enabled significant improvements in signal to noise ratio.[4] The combination of technology developments led to a new range of Raman spectroscopic microscopes in the 1990s, establishing Raman spectroscopy as a relatively inexpensive bench-top laboratory tool to rival conventional IRIR spectroscopy.

Raman is a scattering technique and can be induced in any wavelength region of the optical electromagnetic spectrum. Whereas IRIR absorption spectroscopy measures transitions in the low energy IRIR region of the spectrum, Raman spectroscopy can be carried out using UV, visible or near- IRIR sources, avoiding the need for non-conventional sample mounting in, for example, potassium bromide (KBr) disks or on calcium fluoride (CaF_2) windows as required for FTIR, although for thin samples contributions to the signal from the substrate can be significant. Its adaptability to common silica fibre probes could lead to *in vivo* diagnostic tools, although this is beyond the scope of this chapter.

Raman spectroscopy is viewed as a complementary technique to IR spectroscopy but has significant advantages for many applications, specifically biological. As will be outlined below, Raman is relatively insensitive to water, whose absorption bands often swamp IR spectra, and therefore has potentially significant advantages for *in vivo* diagnostics. The application of Raman spectroscopy to biomolecules and even tissues was first demonstrated as early as the 1960s,[5–7] and by the mid 1970s biomedical applications were explored.[8] Whole cell and tissue studies have been carried out on a range of pathologies,[9–13] and *in vivo* studies have demonstrated the potential use in diagnostic applications.[14–16] Very recent developments have included developments of Raman technologies to probe tissue biochemistry at a depth of many millimetres, leading to the prospect of *in vivo* diagnostics in harder to reach areas of the body.[17] Further developments in probe and other technologies as well as signal processing techniques will undoubtedly see the fulfilment of this potential.

For a detailed description of the basic principles of Raman spectroscopy, the associated instrumentation and potential for spectroscopic imaging, the reader is referred to some of the many excellent texts in the literature.[18–22] This chapter provides an introduction to Raman spectroscopy and how it is measured. It outlines some experimental considerations specific to biospectroscopy and explores applications from molecular through cellular to tissue imaging for biochemical analysis and disease diagnostics. The complementarities and potential advantages over IRIR spectroscopy [Fourier Transform (FTIR) and Synchrotron Fourier Transform (S-FTIR)] are described. Finally, the future potential of the development of Raman spectroscopy for biochemical analysis and *in vivo* disease diagnostics are projected.

4.3 What is Raman Spectroscopy?

Rayleigh or Mie scattering (elastic scattering) occurs when light scattered from a material is of the same frequency (or energy) as the incident light. Raman scattering (inelastic scattering) is a result of light that is scattered off a molecule or solid such that its frequency (or energy) differs from that of the incident light as a result of the interaction. In Raman scattering the energy increase (anti-Stokes) or decrease (Stokes) from the excitation is related to the vibrational energy spacing in the ground electronic state of the molecule, and therefore the shifts in energy of the scattered radiation from the incident frequency are a direct measure of the vibrational energies of the molecule. In Stokes Raman scattering, the molecule starts out in a lower vibrational energy state and after the scattering process ends up in a higher vibrational energy state. Thus the interaction of the incident light with the molecule creates a vibration in the material. In anti-Stokes scattering, the molecule begins in a higher vibrational energy state and after the scattering process ends up in a lower vibrational energy state. Thus a vibration in the material is annihilated as a result of the interaction. The frequency (or energy) differences between the Raman lines and the incident line are characteristic of the scattering molecules and are independent of the frequency of excitation. The process is often depicted as in Figure 4.1 with the aid of a virtual or polarized electronic state. It should be noted however that no electronic transition or "absorption" process is required. The Raman effect arises from the coupling of the induced polarization of scattering molecules (which is caused by the electric vector of the electromagnetic radiation) with the molecular vibrational modes.

Figure 4.2 shows a typical Raman spectrum for crystalline silicon. The parameter of interest is the frequency shift (directly proportional to the energy captured by or donated to the molecule of interest) from the laser illumination, and therefore the incident laser frequency is set to zero, the Stokes line being represented as a positive shift. The Stokes (positive) and anti-Stokes (negative)

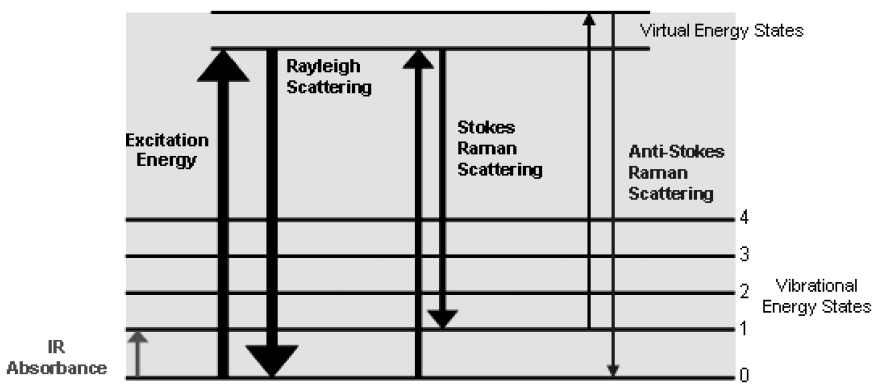

Figure 4.1 Schematic illustration of the transition states during Rayleigh and Raman scattering in a material, in comparison to IR absorption.

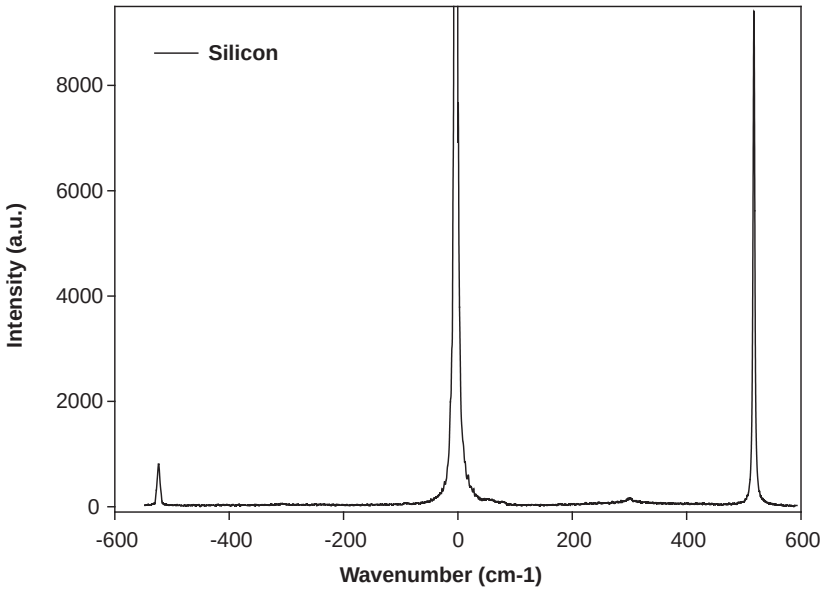

Figure 4.2 Raman spectrum of a silicon crystal showing, from left to right, anti-Stokes, Rayleigh, and Stokes lines. The frequency scale is expressed as the Raman shift with respect to the excitation wavelength; this is why the Rayleigh scattering is at $0\,\mathrm{cm}^{-1}$.

AQ1

Raman lines corresponding to the optical phonons can be seen symmetrically shifted from the incident laser line. For ease of comparison to IR spectroscopy, frequency shifts are expressed in wavenumbers (cm^{-1}). The Stokes shift is most commonly measured at room temperatures, as from simple thermodynamics using Boltzmann's equation, there are very few vibrations in most materials at room temperature which can contribute to anti-Stokes scattering.

At room temperature, the number of molecules in an excited vibrational state will be low. This can be shown by using Boltzmann's equation:

$$\frac{N_V}{N_0} = \exp\left(-\frac{E_V}{kT}\right) \tag{4.1}$$

where N_V/N_0 is the fraction of molecules in the vibrational state; E_V is the energy of the vibrational state; k is Boltzmann's constant and T is the absolute temperature. For example the C=C stretch oscillation ($1612\,\mathrm{cm}^{-1}$ shift) of a benzene ring requires 1.99×10^{-20} Joules of energy to excite the oscillation from the ground state. Using the above equation, the fraction of benzene molecules in the excited vibrational state at 20 °C is 0.0078. Hence it is obvious that, at room temperature, incident photons are much less likely to encounter molecules in an excited state. Therefore the likelihood of Stokes radiation, whereby the molecule captures a portion of the incident photon's energy, is that much

greater than the alternative anti-Stokes, since the anti-Stokes radiation can only occur if the molecule is in an excited vibrational or rotational state. The relative signal strengths of the Stokes to anti-Stokes scattering will change with the temperature of the probed material, and indeed can be used as a measure of temperature.

The Raman effect can be induced by light of all frequencies. However, the cross-section for an inelastic scattering process is proportional to λ_{in}^{-4}, where λ_{in} is the wavelength of the incident photon. For example, photons of 300 nm wavelength have a cross-section of scattering sixteen times greater than photons at 600 nm, assuming that there are no resonance effects, which may occur for incident photons having energy near an electronic absorption line of the molecule.

In a simplified diatomic molecule, in the harmonic oscillator approximation, as in the case for IRIR spectroscopy, the frequency of vibration is given by:

$$\omega_k = (k/m_r)^{1/2} \tag{4.2}$$

where ω_k is the frequency of the vibration, m_r is the reduced mass, calculated by $m_1m_2/m_1 + m_2$, where m_1 and m_2 are the masses of the bonded atoms respectively, and k is the force constant of the vibration, related to the bond energy. In a complex molecule, the vibration of each bond can couple to the incident photons generating a vibrational spectrum on both the Stokes and anti-Stokes sides. As in IR spectroscopy, the frequency positioning of a Raman band is characteristic of a molecular bond or group vibration and the combination of bands represents a characteristic fingerprint of that molecule. It follows that any changes to the fingerprint can be used to monitor or characterize physical or chemical changes at a molecular level.

Not all vibrational modes are "Raman active", however, and the strength of the scattering or the scattering cross-section is governed by selection rules. Whereas electric dipole transitions of IRIR (and UV–visible) absorption require a change of the dipole moment of the material as a result of the transition, Raman scattering requires a change in the polarizability of the bond as a result of the transition. Thus, while Raman spectroscopy is based on a very different photophysical process to the more frequently used FTIR spectroscopic technique, the two vibrational spectroscopic techniques are, in fact, very complementary. Thus, one has access to molecular level information via two different physical processes. In a molecule with a centre of symmetry, a change in dipole is accomplished by loss of the centre of symmetry, while a change in polarizability is compatible with preservation of the centre of symmetry. In a centrosymmetric molecule, asymmetric stretching and bending will be IR active and Raman inactive, while symmetric stretching and bending will be Raman active and IR inactive. In this case, IR and Raman spectroscopy are mutually exclusive. For molecules without a centre of symmetry, each vibrational mode may be IR active, Raman active, both, or neither. Symmetric stretches and bends, however, tend to be Raman active. Vibrations that are strong in an IR

spectrum, those involving strong dipole moments, are usually weak in a Raman spectrum. Likewise, those polarizable but non-polar vibrations that give very strong Raman bands usually result in weak IR signals.

As a crude rule of thumb, those modes that are not Raman active tend to be IR active. By extension, symmetric modes tend to be stronger in Raman than in IR spectroscopy and *vice versa*. For example, hydroxyl or amine stretching vibrations, and the vibrations of carbonyl groups, are usually very strong in an FTIR spectrum, and usually weak in a Raman spectrum. However, the stretching vibrations of carbon double or triple bonds and symmetric vibrations of aromatic groups are very strong in the Raman spectrum. In terms of biochemical analysis, Raman has the particular advantage of minimal interference from the highly polar water vibrations so is a good choice for biological samples with a view to live conditions and *in-vivo* measurements.

Figure 4.3 shows, for example, the Raman spectrum of the amino acid phenylalanine with illustrative band assignments. Particularly strong in the spectrum is the stretch of the highly polarizable aromatic ring at $1004\,cm^{-1}$, also called ring breathing mode. This feature is seen prominently in all Raman spectra of cells and tissue. Figure 4.4 shows the Raman spectra of the amino acids arginine and lysine, and the dipeptide formed between them. Notable is the emergence of the band at $\sim 1650\,cm^{-1}$, the so called Amide I band, common to all peptides and proteins.

Since its discovery in 1928, Raman spectroscopy has evolved in terms of the fundamental understanding of the process, instrumentation and applications. More advanced techniques such as Resonant Raman Spectroscopy (RRS)[22–24]

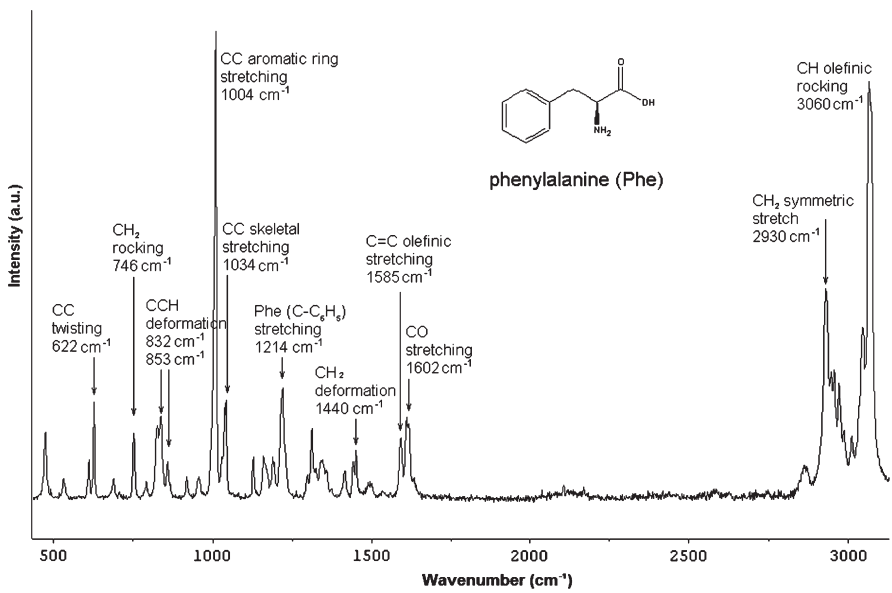

Figure 4.3 Raman spectrum of phenylalanine powder.

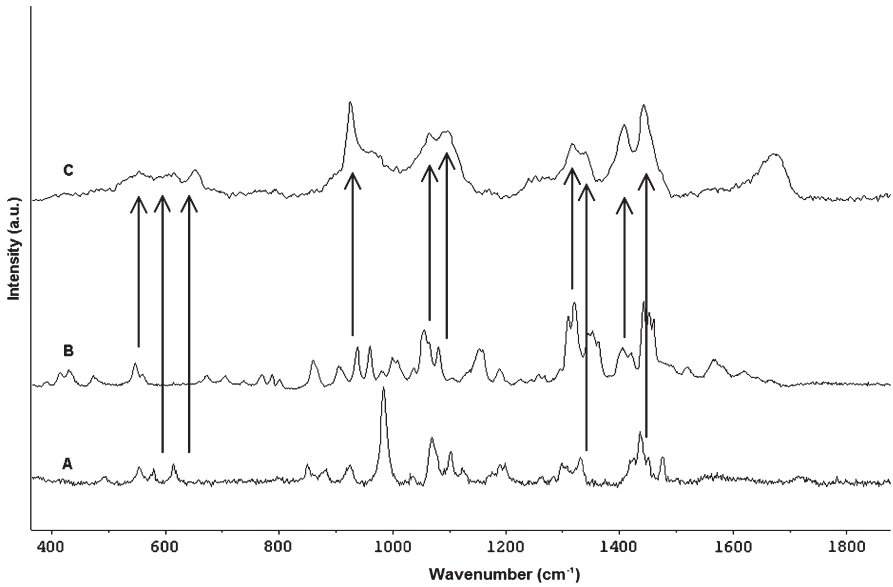

Figure 4.4 Raman spectrum of a A) arginine powder, B) lysine powder, C) dipeptide formed between arginine and lysine.

have found many applications in photophysics and photochemistry. As substrates and media for Surface Enhanced Raman Spectroscopy (SERS)[25,26] are becoming more reliable and reproducible, the technique is finding increased applications for biological, chemical and bioanalytical characterization with high sensitivity and hence low detection limits.[27,28] More advanced techniques such as Coherent Anti-Stokes Raman Spectroscopy (CARS),[29] Stimulated Raman Spectroscopy (SRS),[30] and Hyper Raman Spectroscopy (HRS)[31] have evolved. Although these are extremely powerful techniques in their own right, their increased technical complexity renders them, at present, beyond the realm of routine diagnostic applications, and therefore they are considered beyond the scope of this chapter. In the following sections the basic instrumentation, applications to biospectroscopy and diagnostics and the underlying advantages and drawbacks of Raman spectroscopic microscopy will be discussed.

AQ6

4.4 How is Raman Scattering Measured?

In its most simple form, Raman spectroscopy is implemented using a monochromatic light source, a dispersion element and a light detector (Figure 4.5a). Modern day instruments utilize a laser source, either gas (*e.g.*, Helium–Neon, Argon Ion) or increasingly the more easily miniaturizable solid state lasers (semiconductor diode, titanium sapphire). Depending on the wavelength, powers of 10's to 100's of mW are typically employed. Particularly in the case

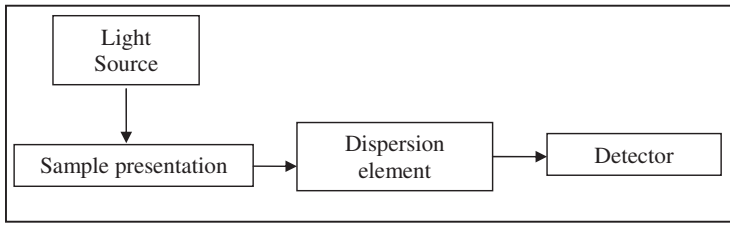

(a)

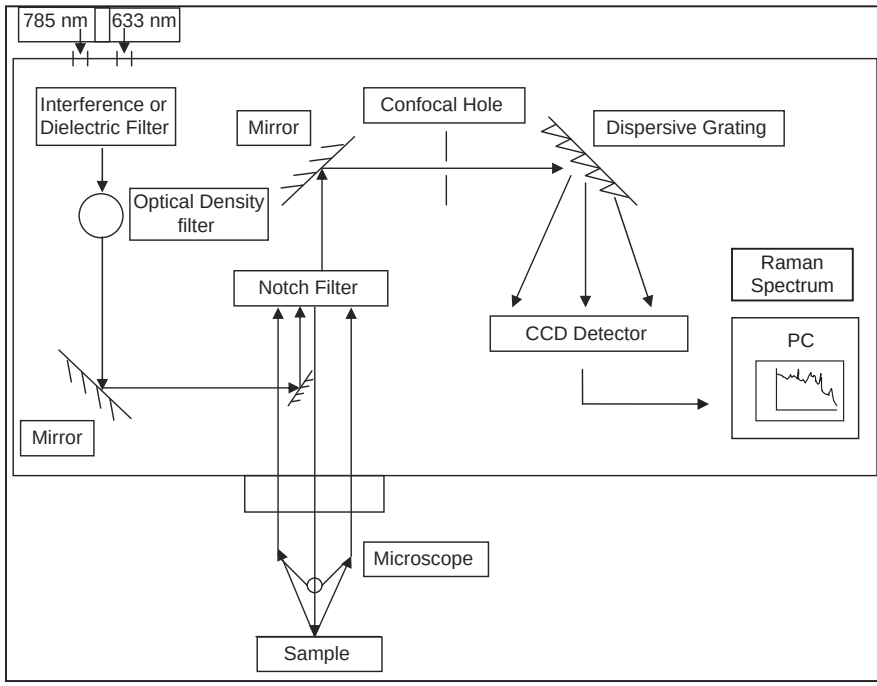

(b)

Figure 4.5 a) Typical set-up for Raman spectroscopy. b) Schematic optical layout of a Raman microspectrometer.

of gas lasers, it is imperative that the background plasma emission in the region of the laser line is minimized such that the weak Raman scattering can be observed and so a dielectric interference filter is used to clean up the excitation line.

The laser is directed onto the sample via a focusing lens, which in modern day systems is usually a microscope objective, often that of a commercially manufactured instrument (*e.g.*, Olympus, Leica, Nikon). Such an instrument allows a selection of objectives from the turret with varying magnification and numerical aperture and, for example, long working distances. With an objective

of $\times 100$, small spotsizes and micron level spatial and axial resolutions are achievable. The spot size is diffraction limited in a similar way to FTIR microspectroscopy, although the significantly shorter wavelength used in Raman spectroscopy leads to significantly higher spatial resolution than those available with IR radiation. The lateral resolution in the diffraction limit is given by:

$$D_x = D_y = 0.61\lambda/NA \tag{4.3}$$

where λ is the wavelength of the light and NA is the numerical aperture of the objective employed. Increased spatial resolution is therefore achievable with shorter wavelengths (UV) and high numerical aperture objectives.

In commercial microspectrometers, the Raman signal is generally collected in a backscattering geometry (Figure 4.5b); the microscope objective which delivers and focuses the laser also acts as the collection lens and collimates the reflected, Rayleigh and Raman scattered light. The collection efficiency is dependent on the numerical aperture of the objective. High numerical aperture is associated with high magnification objectives and therefore small spotsizes and high spatial resolution. Typically, spatial resolution can range from 0.5 μm to 1–2 μm when going from visible to near-IR lasers. Scattered light is collected from the focal depth of the objective and thus the choice of objective also governs the sampling depth in transparent materials. A high magnification objective gives a surface sensitivity (in transparent materials) of ~ 1 μm, while a longer focal length $\times 10$ objective can be used to sample the depth of a transparent liquid or solid (Figure 4.6).

The resolution in the z-direction is given by:

$$D_z = \lambda n/(NA)^2 \tag{4.4}$$

where n is the refractive index of the medium between the lens and the sample.

Raman microscopes commonly operate in a confocal mode. Confocality has the advantage of providing improved z-resolution and better discrimination of the Raman signal from diffusely scattered radiation in inhomogeneous materials such as tissue. Before entrance to the spectrometer, the collimated radiation is imaged onto a variable aperture. The imaged spotsize is typically ~ 100–200 μm, and radiation not emanating from the focal region of the microscope objective, or which is diffusely scattered by the sample, is blocked by the confocal hole, providing better depth resolution and discrimination of the Raman signal from other radiation.

Once collected, it is important to remove the strong contributions from the reflected or Rayleigh scattered laser light. This is commonly achieved using a holographic Notch filter or a dielectric stack (Figure 4.7) which has a spectrally narrow reflection band centred on the laser wavelength. The element acts as an almost 100% reflector of the laser radiation, which directs it into the microscope for illumination. The collimated backscattered radiation is incident on the element on its return, whereupon the reflected and Rayleigh scattered

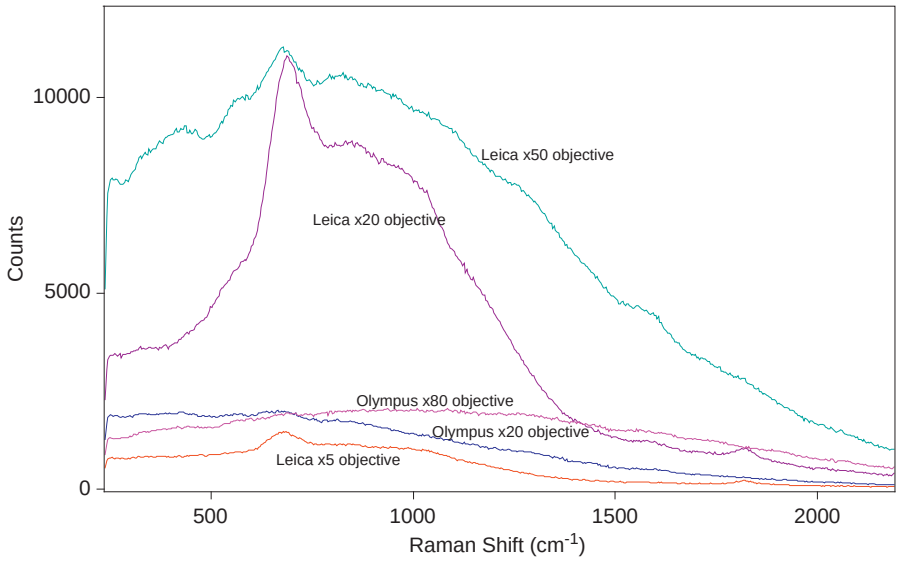

Figure 4.6 Collection optics for Raman spectroscopy in the backscattering geometry. A comparison of spectral contributions from different illumination/collection optics. The spectra were excited from a clean chromium surface at 830 nm excitation (32 mW) and with an integration time of 30 s.

radiation is reflected, while the frequency shifted Raman bands are transmitted into the spectrometer. The spectral width of the element can be tailored to differing specifications but typically the Raman signal can be recorded to within 50–100 cm^{-1} shift from the laser line. This routine specification is a significant improvement over the spectral responses of commercial FTIR systems in the far-IR region which typically have a lower limit of $\sim$400 cm^{-1}.

The transmitted radiation is spectrally dispersed using a diffraction grating. The grating can be optimized for the operating wavelengths but typical gratings cover the entire optical range.

Commonly, instruments are fitted with two or more interchangeable gratings to allow for low or high resolution measurements, covering the spectral range of interest in a single image or multiple images which can then be "stitched" using the instrument software. Operating at low resolution allows more rapid spectral recording and improves the signal to noise ratio by increasing the signal per wavenumber interval. Higher dispersion gratings can be employed where the fine structure of spectral features is to be resolved (*e.g.*, the Amide I band of proteins which gives information on secondary structure and conformation).

Spectrometer lengths are typically 300 mm for medium resolution or 800 mm for high resolution systems. The dispersion per pixel is thus typically 1 cm^{-1} for a 300 mm length spectrometer with an 1800 mm^{-1} grating operating at 633 nm and can be as low as 0.25 cm^{-1} for a high resolution system. The resolution of

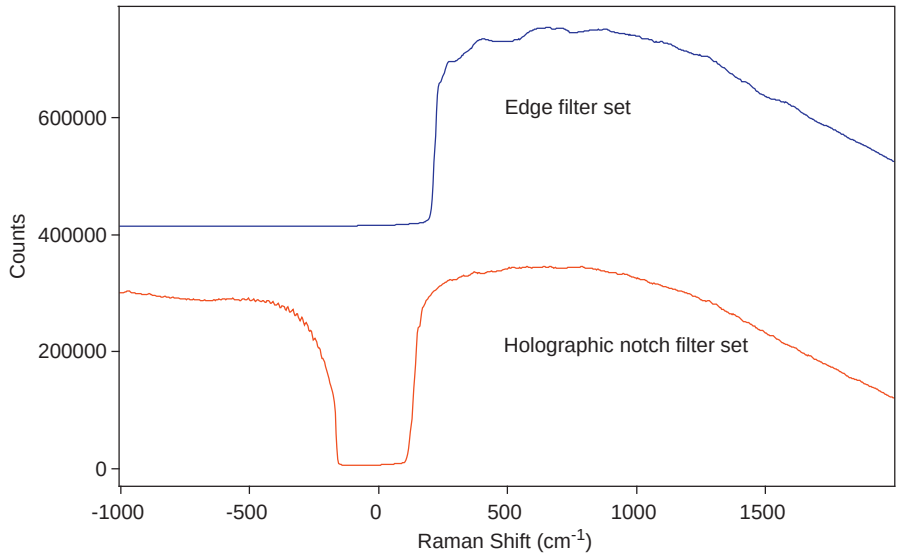

W-filament lamp spectrum measured with each filter set.

(a)

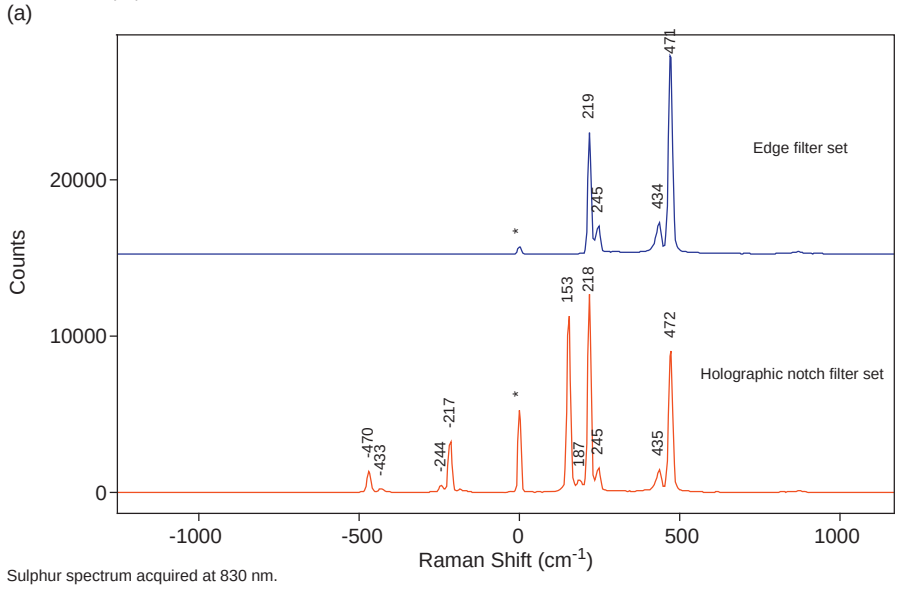

Sulphur spectrum acquired at 830 nm.

(b)

Figure 4.7 a) Comparison of white light spectra measured with a spectrometer fitted either with an edge filter set or a holographic notch filter set. Spectra were acquired for 60 s. The y-axis has arbritary units of intensity, whereas the x-axis represents the spectral energy in cm^{-1} relative to 830 nm ($0\,cm^{-1}$). b) Comparison of sulfur spectra measured at 830 nm, with a Raman spectrometer fitted either with edge filter or holographic notch filter sets. c) Spectral contributions from some typical optical substrates at 830 nm, with 32 mW laser power at the sample, ×80 objective, t = 10 s.

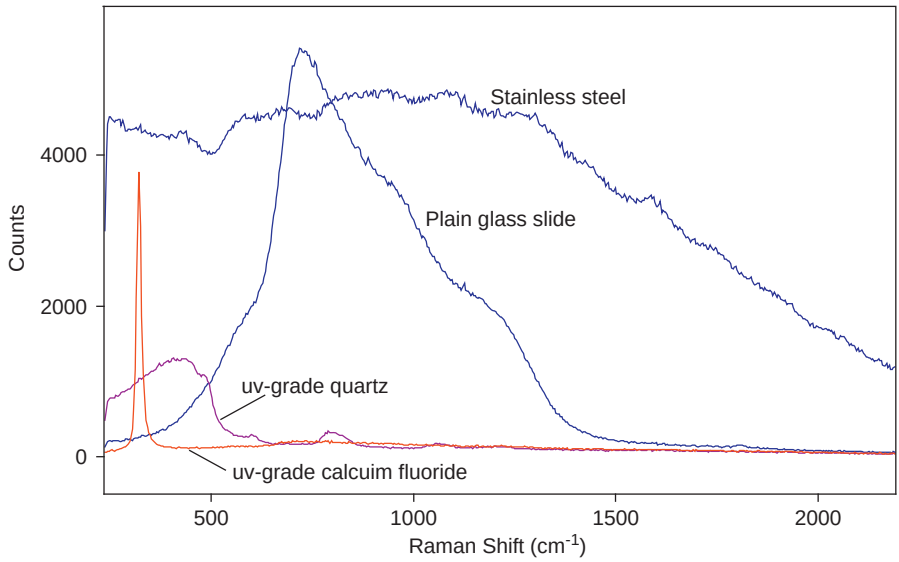

Spectral contributions from backing substrates at 830 nm

(c)

Figure 4.7 Continued.

the spectrometer is of course additionally determined by the entrance optics, and commonly instruments are fitted with a variable entrance slit. For comparison, commercial FTIR instruments commonly operate at 2–16 cm^{-1} resolution and high resolution systems can achieve resolution for gas spectroscopy. The spectral resolution depends mainly on the displacement of the moving mirror of the interferometer.

The Raman signal is commonly collected using a charge coupled detector (CCD) device. Many different CCD options are available on commercial systems, including Deep Depletion CCDs which are required for the near-IR region, Back Thinned CCDs which can increase sensitivity, and electronic amplified CCDs which can increase the signal but also the noise. Recent improvements in CCD sensitivities mean that sufficient signal to noise can be achieved using electronic Peltier cooling, avoiding the inconvenience of cryogenic coolants. The Peltier effect is a thermoelectric effect whereby heat is displaced from a conducting material to another in the presence of an electrical current.

A further feature of modern Raman spectroscopic microscopes is that the laser is polarized, allowing determination of, for example, depolarization ratios, and molecular orientation in crystals or liquid crystals. Care must be taken to account for the polarization response of the vertically ruled diffraction grating however. To date, there have been few or no polarization dependent studies of biological materials although recent studies have demonstrated that polarization dependent Raman can detect structural changes in the extracellular matrix associated with basal cell carcinoma.[32]

The above describes the commonly utilized instrumentation required for dispersive Raman spectroscopic microscopy. In the past, Fourier transform Raman spectroscopy provided an alternative for coloured and fluorescent samples but the use of near-IR lasers at 1.064 μm together with In:Ga:As detectors reduced the sensitivity. Recent developments in laser rejection filters and CCD technologies have rendered dispersive techniques the preferred option.

Similar to conventional IR microscopy (mapping in opposition to recent imaging array detectors), Raman spectroscopic microscopy is usually performed as a point measurement, the sample area and depth being determined by the choice of the objective. Because it is an intrinsically weak phenomenon, relatively high power densities are required and simultaneous illumination over large areas and detection by multiple detector arrays, as can be performed with FTIR and Focal Plane arrays, is not easily achieved. To date, therefore, Raman imaging *per se* has been performed as a stepwise mapping process. Average collection times to achieve acceptable signal to noise ratios for materials such as tissue sections can be between ten and several tens of seconds (from low to high excitation wavelengths). Mapping a significant area of even 10×10 μm, with a 1 μm diameter spot, can therefore be a time consuming exercise. Significant effort has therefore been devoted by the instrument manufacturers towards improving sampling rates and mapping capabilities. Line mapping and continuous scanning modes have been introduced in many commercial systems although the weakness of the signals derived from biological samples remains a limiting factor.[33]

4.5 System Calibration

In a dispersive Raman set-up, the spectral dispersion is achieved by the action of a diffraction grating which distributes the light onto the multidetector CCD array. The system software keeps a record of which pixel of the CCD corresponds to which wavenumber of the spectrum. The process of assigning spectral positions to pixel number is one of calibration. The calibration can however change from day to day as the dispersion depends on the optical pathlength (distance times refractive index) between the grating and the detector. Small changes in temperature and/or humidity can thus affect the spectral calibration on a day to day basis and it is important to ensure that a rigorous calibration procedure is adhered to if direct inter-comparison of results is required. It is also important to note that the system sensitivity (intensity response) can vary depending on the laser line employed, the angle of the laser line rejection filter, the grating, the objective, the detector, and many other system parameters. Whereas FTIR spectra are taken as a ratio of the sample spectrum to a reference, no such facility is available in conventional Raman spectroscopy. Contributions due to sample substrate can also influence the results significantly (see Figure 4.7c for the contribution of different optical substrates).

Thus, for intra- and inter-laboratory comparison, it is important to calibrate the intensity axis also. Recommendations from manufacturers vary, and

therefore the DASIM Raman Working Group has devised a calibration protocol based on a consensus of best practice. This protocol is outlined in Addendum A and shown schematically in Figure 4.8. In general, it is important to record the spectrum of the dark response and substrate to be used for the measurements in advance of a measurement set. Figures 4.9a and 4.9b show, respectively, the flowchart and an example of the Raman pre-processing procedures.

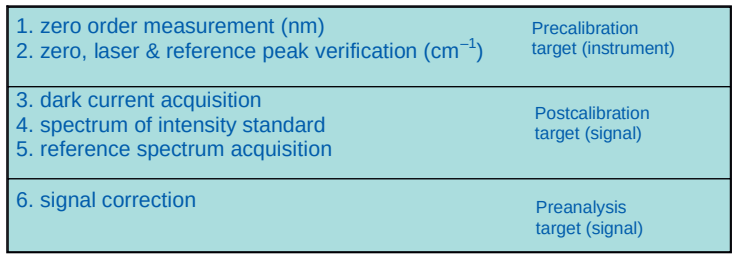

Figure 4.8 Raman calibration procedure.

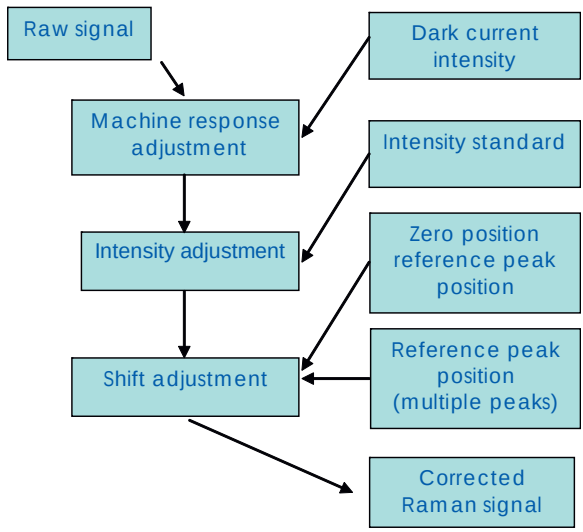

Figure 4.9 (a) Flow-chart showing Raman pre-analysis procedure. (b) Step 1 showing the subtraction of dark current from the raw Raman spectrum and the white light signal and the ration of the former to the latter to give a first corrected spectrum. (Courtesy of C. Gobinet.) (c) Step 2: starting from the corrected spectrum in step 1, the spectrum is smoothed, then the substrate and background are subtracted to give the final spectrum corrected for both instrument response and substrate contribution. (Courtesy of C. Gobinet.)

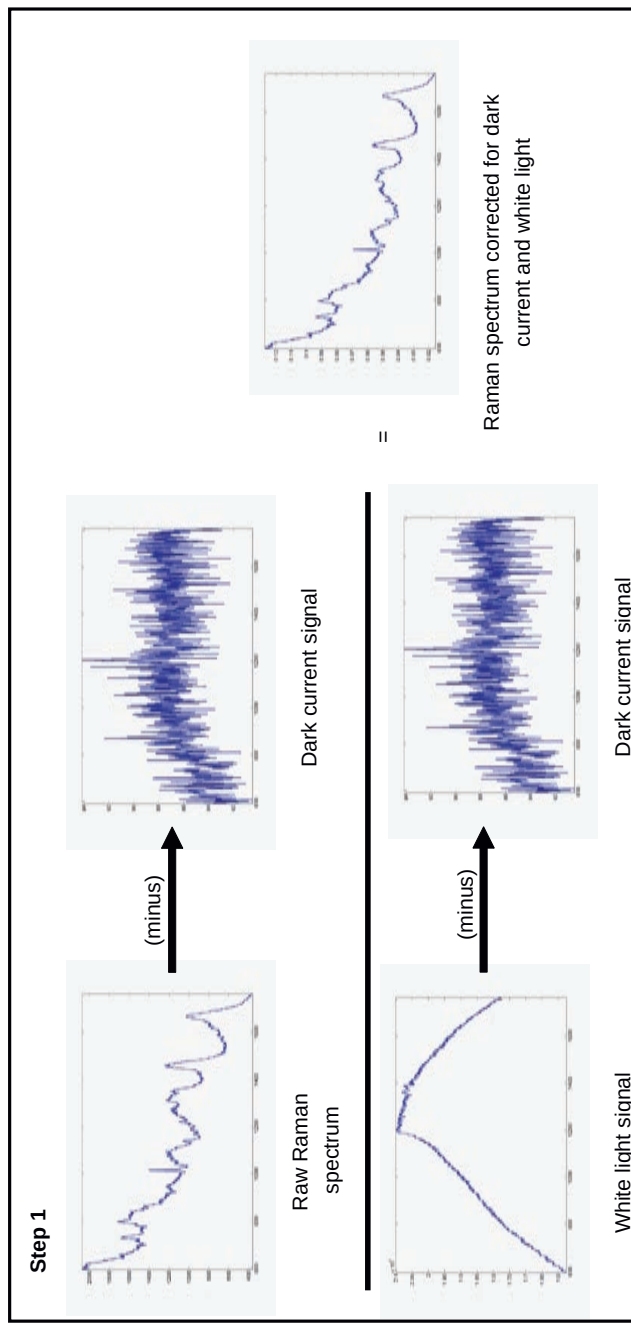

Figure 4.9 b) Continued.

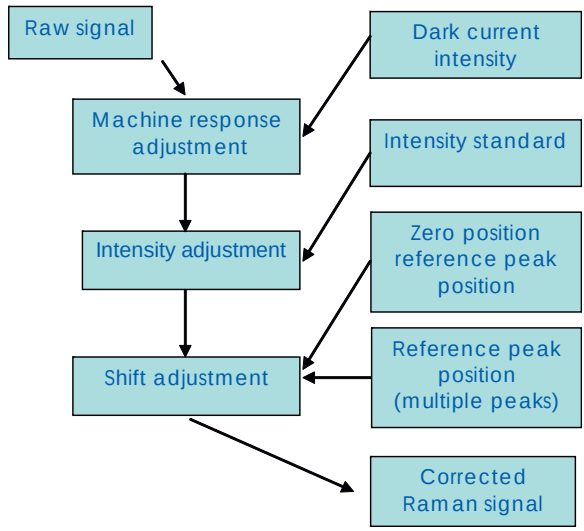

Figure 4.9 (c) Continued.

Figure 4.9b and 4.9c show a two-step procedure. Step 1 shows the subtraction of the dark current from both the raw Raman spectrum and the dark current spectrum. The former is then divided by the latter to give in the first instance a Raman spectrum corrected for dark noise and white light. Step 2 considers the latter spectrum and includes a Savitsky–Golay smoothing, followed by subtraction of the substrate (here quartz) and the background contributions (here a fourth order polynomial). The final Raman spectrum is thus corrected for instrument response and substrate contribution.

4.6 Raman Spectroscopy for Diagnostics and Biochemical Analysis

Raman (micro)spectroscopy has the advantage of finding applications going from isolated molecules, complex systems like macromolecules, cells, tissues, to humans. Applications of Raman spectroscopy to disease diagnostics and biological analysis are numerous and varied. The following outlines one study as an example.[34]

AQ2

FFPP cervical tissue sections were characterized by the Registrar, National Maternity Hospital, Holles St, Dublin; the samples consisted of 20 normal and 20 invasive carcinoma sections from 40 individuals. Of the 20 carcinoma samples, 10 samples were identified as having various grades of cervical intraepithelial neoplasia (CIN), which were also marked for examination. Figure 4.10 shows the different cell types seen in normal cervical tissue in an unstained FFPP tissue section together with the Raman spectra recorded from basal cells, epithelial cells, and connective tissue. Spectra were recorded from a

single sample and each spectrum represents a different spot within the sample. The spectra of the three different cell types do have a degree of similarity as seen previously for different tissue types. However, there are also many spectral features differentiating the different cell types. The spectra of basal cells show strong bands at 724, 779 and 1578 cm^{-1} which are characteristic of nucleic acids (Figure 4.10A). The same contributions were observed in the spectrum of

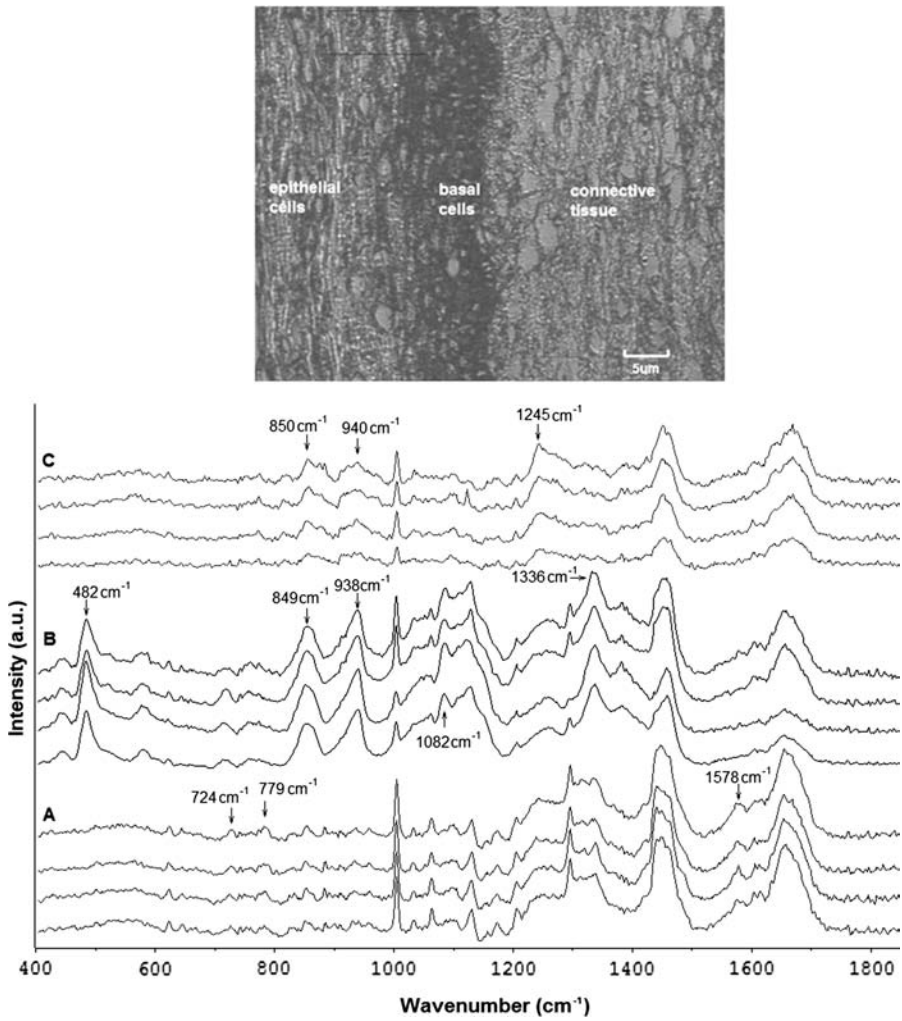

Figure 4.10 Left: Photomicrograph of unstained cervical tissue section, with different cell types identified. Right: Micro-Raman spectra recorded from basal cells (A), epithelial cells (B), and connective tissue (C) in cervical tissue sections. The main spectral features associated with each cell type are highlighted.

DNA. The morphology of basal cells consists of a single line of tightly packed cells, with large nuclei in relation to the compacted surrounding cytoplasm. In addition, these cells are constantly dividing, providing cells to the parabasal layer. For both of these reasons, a high concentration of DNA would be expected in the basal cells. Spectra of epithelial cells have characteristic glycogen bands at 482, 849, 938, 1082 and 1336 cm^{-1} (Figure 4.10B) as observed in the spectrum of glycogen. Collagen contributions can be clearly seen in the spectra of connective tissue at 850, 940 and 1245 cm^{-1} (Figure 4.10C).

Figure 4.11a compares the Raman spectra collected from normal epithelial cells and invasive carcinoma from a selection of different patients. Glycogen contributions are clearly visible in the spectra from the normal epithelial tissue. The most obvious bands arise at 482, 849 and 938 cm^{-1} and are due to glycogen skeletal deformation, CCH aromatic deformation and CCH deformation respectively. However, there are also other glycogen contributions not as apparent, including a CC stretching band at 1082 and CH_3CH_2 wagging at 1336 cm^{-1}. These glycogen bands (482, 849 and 938 cm^{-1}) are absent in the spectra from invasive carcinoma, as well as a reduction in the intensity of the CC stretching mode (1082 cm^{-1}). Glycogen is known to be linked with cellular maturation and disappears with the loss of differentiation during neoplasia.[35] This agrees with the findings in other Raman and FTIR studies of epithelial tissues. The spectra of invasive carcinoma also show characteristic nucleic acid bands. These include prominent bands at 724, 779 and 1578 cm^{-1}, but also at 829, 852, 1098 and 1240 cm^{-1}. Distinct bands were also seen at 1366 cm^{-1}, a shoulder at 1484 cm^{-1} and a band at 1578 cm^{-1}. An increase in the intensity of the Amide I band (1655 cm^{-1}) was also observed in the spectra of carcinoma samples compared to the normal tissue samples. The increased nucleic acid and protein bands are a result of the increased proliferation of these tumour cells.

To investigate whether pre-malignant changes could be highlighted using Raman spectroscopy, 10 areas of neoplasia (CIN) from 10 different patients were marked by a pathologist and a selection of the resulting Raman spectra are shown in Figure 4.11b. A number of the spectral features identified in the invasive carcinoma samples were also observed in the CIN samples, such as the nucleic acid bands at 724, 779, 852, 1366 and 1578 cm^{-1}. This indicates that early biochemical changes can be identified using Raman spectroscopy.

Principal components analysis was used to reduce the number of parameters needed to represent the variance in the spectral data set. The principal components were then used to generate a linear discriminant model. All three tissue classes were successfully discriminated as shown in Figure 4.12. The classification model was tested using a leave one out cross-validation in which all but one spectrum were used to build the model. This model was then used to predict the remaining spectrum. This was repeated for all 498 spectra. Of 498 tissue spectra, 492 were correctly classified as normal, invasive carcinoma or CIN. The cross-validation misclassified six spectra, two of which

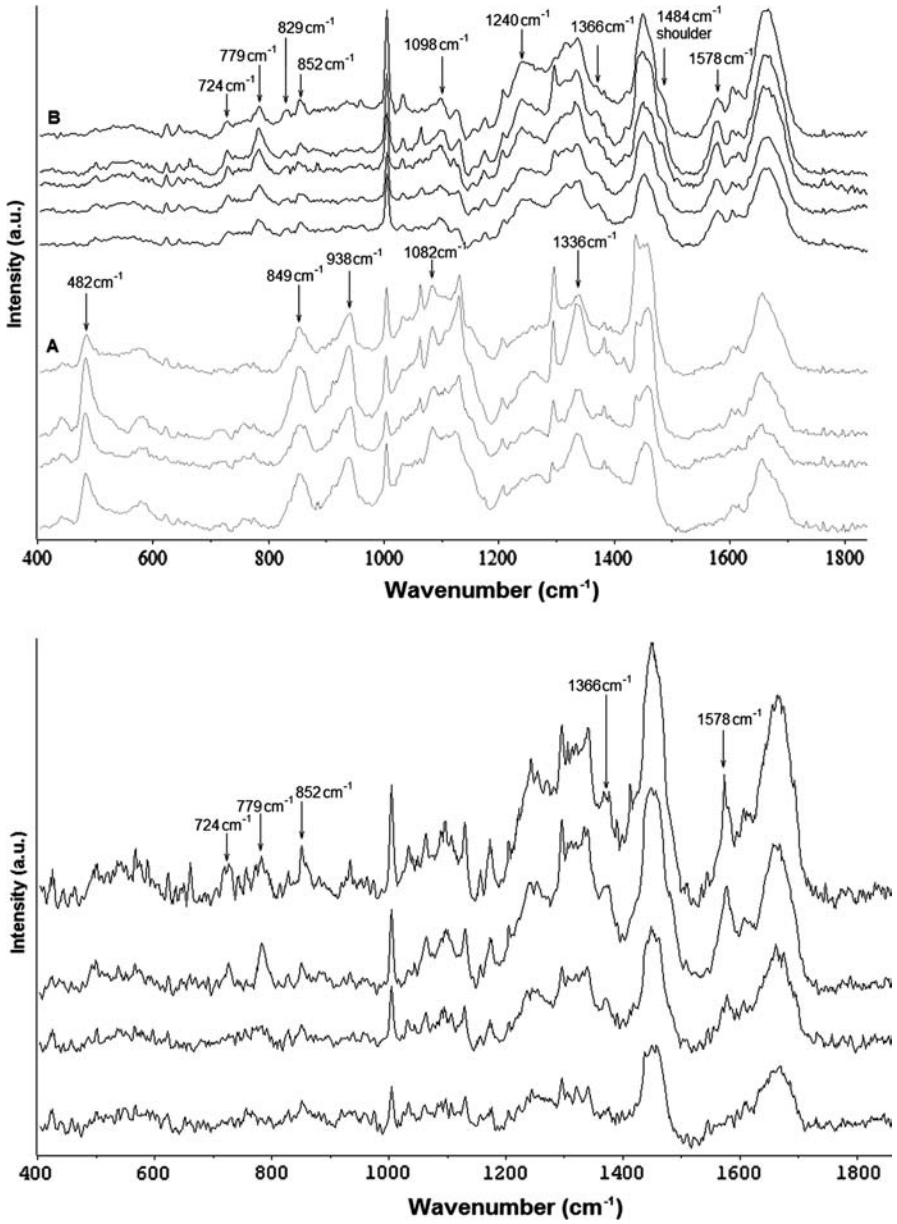

Figure 4.11 Raman spectra of a) normal cervical epithelial cells and invasive carcinoma cells, and (b) Raman spectra of cervical intraepithelial neoplasia (CIN) tissue. Assignments of the main Raman vibrational modes are detailed in Table 4.1, below.

Table 4.1 Peak position and assignments of main Raman vibrational modes.

Peak position (cm^{-1})	*Assignment*
622	C–C twisting
724	CH_2 deformation
746	CH_2 rocking
754	Symmetric ring breathing
779	Ring vibration
832	CCH deformation aliphatic
853	CCH deformation aromatic
873	CC stretch
922	C–C stretching
1004	CC aromatic ring breathing
1034	C–C stretching
1065	C–N stretch
1096	C–C chain stretching
1098	CC stretch
1102	CC stretch
1124	CC skeletal stretch *trans*
1214	CC stretch backbone carbon phenyl ring
1236	CN stretch, NH bending Amide III band
1240	CN stretch, NH bending Amide III band
1314	CH deformation
1337	CH_2 deformation
1335	CH_2 deformation
1366	CH_2 bending
1440	CH_2 scissoring
1484	CH_2 deformation
1548	NH deformation; CN stretch Amide II band
1578	C=C olefinic stretch
1585	C=C stretching
1602	CO stretching
1660–1665	C=O stretch Amide I α-helix
2930	CH_2 stretching ($2930\,cm^{-1}$)
2932	CH_3 symmetric stretch ($2932\,cm^{-1}$)

were normal samples assigned as invasive carcinoma. The other four were either invasive carcinoma or CIN misclassified as either CIN or invasive carcinoma respectively. Importantly, no abnormal samples were classified as normal. Based on the cross-validation results, sensitivity and specificity values were calculated as 99.5% and 100% respectively for normal tissue, 99% and 99.2% respectively for CIN and 98.5% and 99% respectively for invasive carcinoma.

The results show the ability of Raman spectroscopy to classify cervical cancer and pre-cancer with high sensitivity and specificity. These classifications are based on biochemical changes known to accompany cervical cancer such as loss of differentiation and increased proliferation. This study shows the capability of Raman microspectroscopy to investigate not only the tissue but also the cells within the tissue, as it is known that a tumour can contain a heterogeneous population of cells.

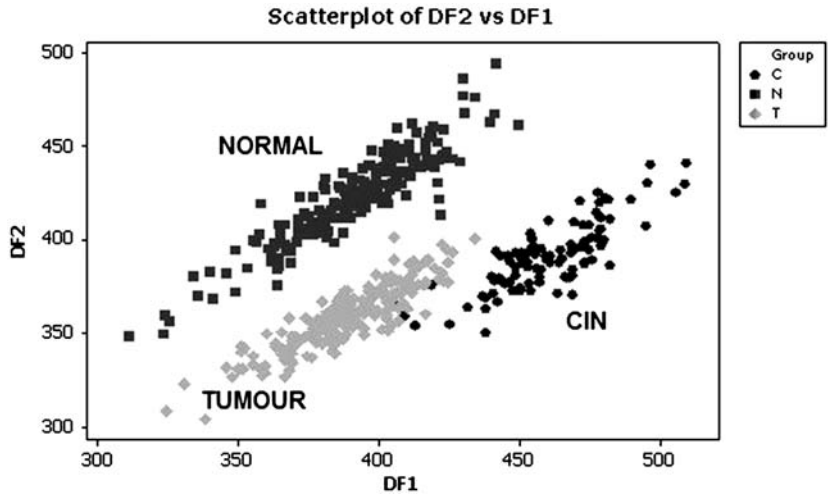

Figure 4.12 Linear discriminant analysis of the principal components of the first derivative, normalized, 10 point averaged spectra, over the entire spectral range. **C** = CIN, **N** = normal and **T** = invasive carcinoma.

4.7 Raman Microscopy and Imaging at Cellular and Subcellular Levels

The possibility of probing events at the single cell level is of great importance in disease diagnostics, in particular for cancer. Single cell analysis is an important issue both on a fundamental level, for understanding biological processes such as cell differentiation and proliferation, cell division and cell death, and on a clinical level for rapidly assessing cell phenotype or how a patient will respond to a given drug treatment. Very often, in real life samples, only a few cells are available for diagnostic purposes. Given the importance of developing non-invasive, cell-specific detection and monitoring methods, researchers are encouraged to develop low-cost, widely accessible, real-time detection and sensing technologies for living systems. Thus there is a real need for techniques capable of probing single cells. However, there are not many existing methods that can give access to high biomolecular information with cellular and sub-cellular resolution. Raman and IR microspectroscopies have such potential, as they can give spatially resolved biochemical information without the use of extrinsic labels and without being invasive or destructive to the studied system. Both IR and Raman techniques are truly label-free since the inherent vibrational signatures of the biochemical components of a cell are being observed. A significant advantage of Raman spectroscopic microscopy over FTIR microscopy is that of lateral spatial resolution. The micron- or submicron-level spatial resolution obtained with lasers and adapted optics helps to interrogate subcellular compartments. Furthermore, Raman techniques can be readily applied to single live[36] and fixed[37] cells.

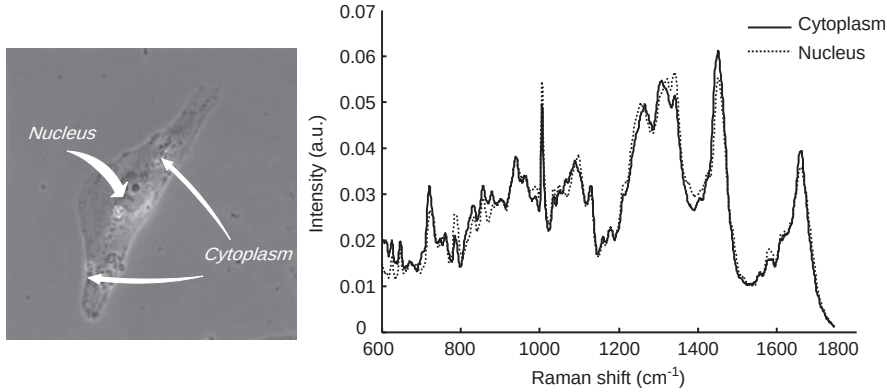

Figure 4.13 Photomicrography showing a single live cancer cell growing on a quartz window and the cellular compartments such as the nucleus and cytoplasm. Micro-Raman spectra corresponding to these compartments measured with an ×100 water immersion objective, 50 mW of a 785 nm laser, and a collection time of 20 s. (Courtesy of F. Draux.)

Raman spectroscopy has proven its potential for the analysis of cell constituents and processes. However, sample preparation methods compatible with clinical practice must be implemented for collection of accurate spectral information. Micro-Raman spectroscopy as a non-invasive and non-destructive tool can therefore probe single living cancer cells while preserving cell integrity and functions, such as adhesion and proliferating capacities.[36] Figure 4.13 shows an example of micro-Raman spectra recorded from the nucleus and cytoplasm of a single live cancer cell using a 785 nm laser excitation and a ×100 water immersion objective. It highlights the differences in the biochemical and molecular composition between the cytoplasmic and nuclear cell compartments. Such spectral data are then compared in order to identify spectral signatures of the main macromolecules such as nucleic acids, lipids and proteins. Table 4.2 shows the main Raman bands observed when exciting the cells with a 785 nm laser. Based on these signatures and using multivariate statistical approaches, Raman maps of a single living cancer cell can thus be produced. Thus, Raman spectral imaging at the single living cell level represents a potential avenue for probing various cellular processes and monitoring for example cell–drug interactions. It can be developed into a rapid, high throughput, and automated diagnostic tool for screening cells from patients.

On a fundamental research basis, and as a complement to FTIR spectroscopy, Raman spectroscopy can be used to understand the processes underlying cancer cell migration (metastasis) in model systems mimicking the extracellular matrix or the cancer cell's microenvironment.

Efforts to measure single cells in aqueous media by synchrotron IR microscopy in a flow system have been attempted but remain challenging.[38] However, in a study to monitor the response of cancer cells to an antitumour drug, it was shown that results obtained using synchrotron FTIR microscopy of fixed single

Table 4.2 Some of the major peaks that can be observed in the Raman spectrum (excitation at 785 nm) of single cells.

Wavenumbers	*Assignments*
787	DNA/RNA: ring breathing (C)
809	RNA: O-P-O stretching
1003	Prot: ring breathing Phe
1092	DNA/RNA: O-P-O stretching
1264	Prot: Amide III
1451	Prot: (C–H) bending
1486	DNA/RNA: ring mode (G,A)
1553	Prot: c=C stretching (Trp)
1575	DNA/RNA: ring mode (G,A)
1660	Prot: Amide I

cells gave comparable results to bench-top FTIR measurements of cell populations.[39] More recently, ATR-FTIR imaging was used to monitor cancer cell compartments in natural aqueous media.[40] The latter mode may also reach higher spatial resolution down to 2–3 μm when using a high refractive index element like germanium. Combined with a synchrotron source and new imaging detectors, these modalities will open new avenues for applications in cytology as the performances are expected to be comparable to Raman microspectroscopy. It must be noted that with modern micro-Raman systems, live or fixed cells can now easily be probed with green lasers operating at low powers without damaging them and with little or no parasitic fluorescence background.

An increase in the number of applications for single cell analysis is therefore foreseen and this will undoubtedly foster the development of Raman and IR as innovative approaches for spectral cytology. They can be automated into techniques for earlier detection of diseases with enhanced resolution, sensitivity and specificity.

4.8 Comparison to FTIR – Pros and Cons

4.8.1 Physical Principles

Fundamentally, Raman scattering is of different physical origin from IR absorption spectroscopy and many of the pros and cons in terms of applications stem from this fundamental difference and how it impacts on the regions of the spectrum probed, the sample response and the technological implications and limitations. A fundamental difference lies in the fact that Raman is a scattering process originating from a change in the molecule's polarizability whereas IR absorption is an electric dipole transition resulting in the absorption of a photon. The two processes are governed by different selection rules and thus while the two techniques can be considered complementary, the molecular fingerprint of a material obtained from Raman spectroscopy is different from that obtained from IR absorption spectroscopy. Figure 4.14

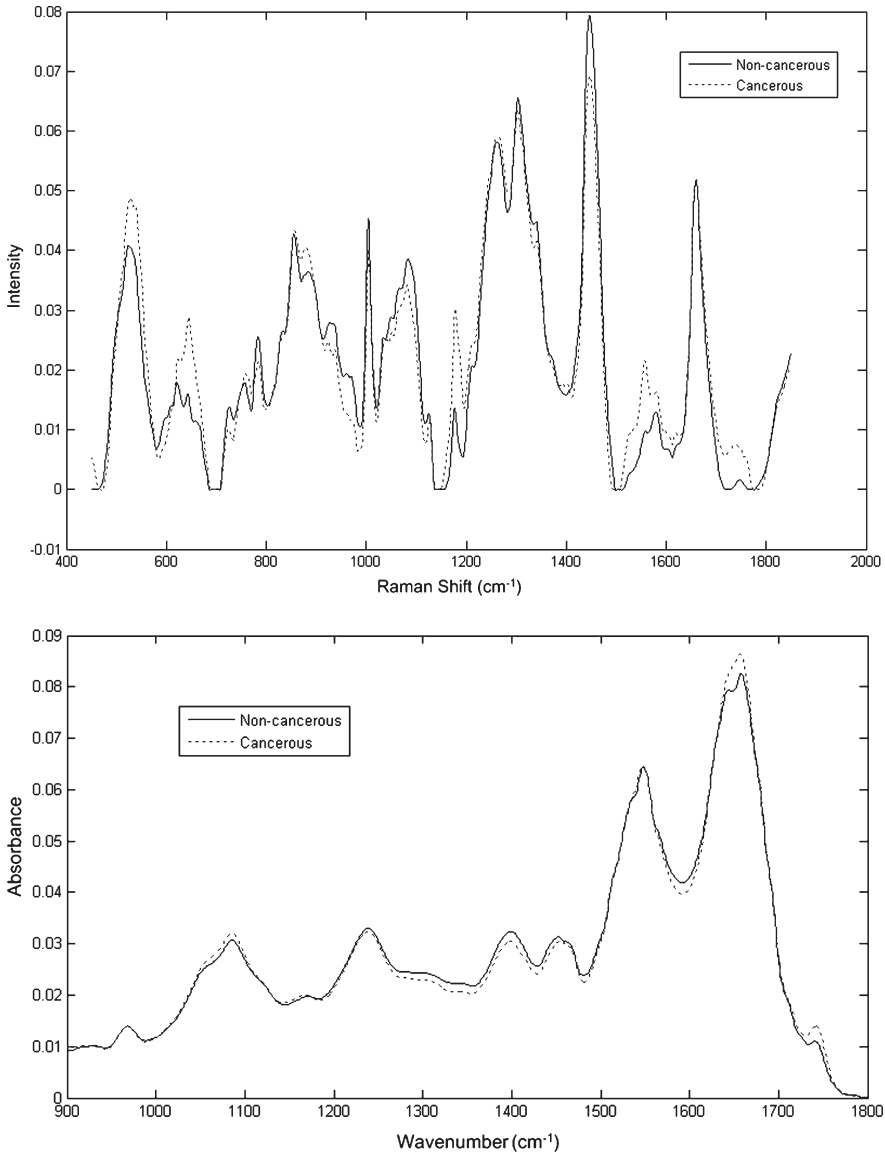

Figure 4.14 Mean Raman (left) and FTIR (right) spectra obtained from oesophageal lymph nodes. Both figures cover the "fingerprint" spectral range, which is the region of both spectra where most spectral features are found.

compares the mean Raman and FTIR spectra of oesophageal lymph nodes, and Table 4.3 lists the peak assignments.

While both are rich in the so-called fingerprint region, it is clear that the Raman spectrum intrinsically contains significantly more information. There

Table 4.3 Key peaks and their assignments observed in Raman and FTIR spectra of lymph nodes.

Biomolecule	*Raman peaks (cm^{-1})*	*Biomolecule*	*FTIR peaks (cm^{-1})*
Protein	**1659**, **1451**, **1319**, **1246**, 1207, 1174, 1128, 1103, 1058, **1002**, 959, **936**	Protein	**1662**, **1646**, **1550**, **1532**, **1516**, 1471, 1453, 1403, 1387, 1238,1171, 979
Nucleic acids	1666, **1574**, 1483, 1459, 1414, 1377, 1336, 1304, 1291, **1253**, 1215, 1194, **1099**, **1066**, 1011,957, **913**	Nucleic acids	**1712**, 1662, 1643, 1602, 1576, 1527, 1493, 1406, 1370, 1327, 1238, 1212, **1088**, **1050**, **1011**, **962**, 917
Fatty acids	1636, 1464, **1441**, 1423, 1375, **1298**, 1175, **1129**, 1099, **1064**, 1029, 1011, 977	Fatty acids	**1705**, **1689**, **1464**, 1431, **1408**, **1311**, **1295**, 1271-1187, 1098, 940
Triglyceride	**1747**, **1653**, **1439**, **1300**, **1267**, 1117, **1079**, 1038	Triglyceride	**1747**, **1466**, **1380**, 1243, 1164, 1118, 1096
Carbohydrates	1461, **1382**, **1337**, 1261, 1207, **1125**, 1084, **1049**, **939**	Carbohydrates	1201, **1153**, **1080**, 1055, **1020**, **994**

are many molecules such as amino acid residues, S–S disulfide bridges, C–S linkages from proteins, and nucleic acid signals that are more highlighted in Raman spectra. This may also result from the significantly higher resolution ($\sim 1\,cm^{-1}$) of typical research grade Raman spectrometers compared to FTIR instruments (~ 2–$8\,cm^{-1}$). The FTIR spectrum exhibits broad features due to overlapping bands. However, it is known that increasing the spectral resolution in IR does not significantly improve the band width. This higher biochemical information content, associated with a higher resolution, affords an ease of differentiation between for example normal and cancerous tissue for diagnostic applications (Figure 4.15). The wealth of information is often highlighted through the use of first or second order derivative spectra.

The key advantage of Raman for *in vivo* diagnostics is the low contribution of water to the Raman signal. Most human tissues contain around 70–80% water. Furthermore, the illumination and scattered light for Raman is usually of ideal wavelengths for transmission through optical fibres. This is certainly not the case for mid-IR light as overcoming the water signal with IR fibre probes is a real challenge.

4.8.2 Spatial Resolution

The spatial resolution of either measurement is determined by the diffraction limit and therefore the wavelength of the light used in the spectroscopic technique, as well as the imaging optics. For visible light (wavelength $\approx 0.5\,\mu m$), this implies that spot sizes as low as 1 μm diameter are easily attainable whereas

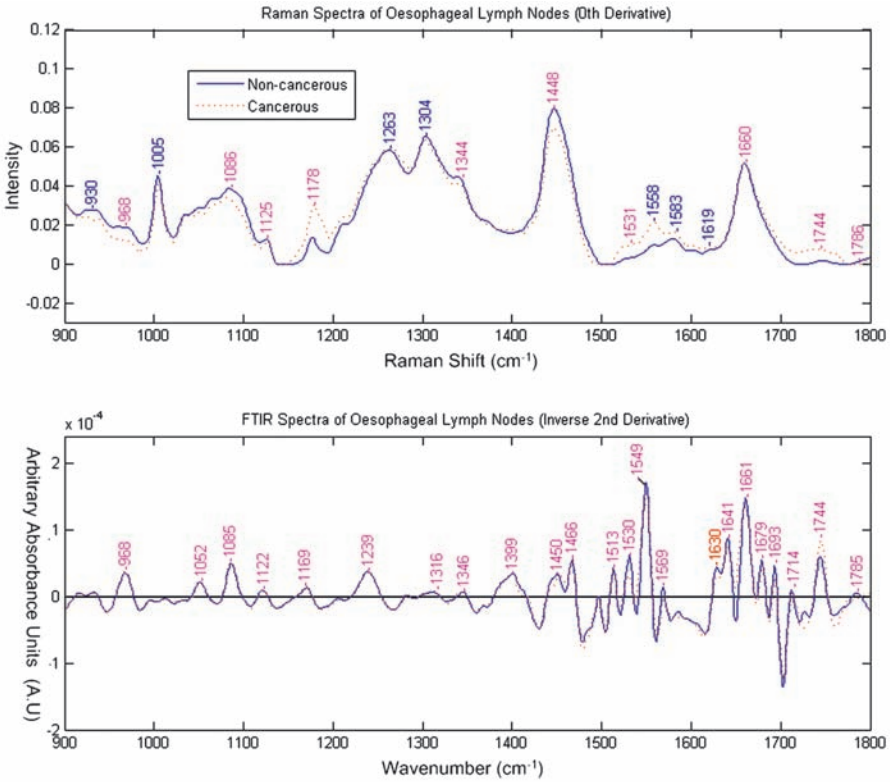

Figure 4.15 Plot of Raman (0^{th} derivative) *vs.* FTIR (inverse 2^{nd} derivative) mean spectra for non-cancerous and cancerous lymph nodes (numbers in purple indicate peaks shared in both Raman and FTIR while numbers in blue are only selective for Raman and those in red only selective for FTIR).

in the mid-IR (wavelength $\approx$5–10 μm) apertured spot sizes of 25 μm are typical with bench-top instruments. At such spatial resolution, subcellular detail is impossible to determine. The DASIM project has helped to advance synchrotron FTIR microscopy at cell and tissue levels. The high brilliance of the source enables apertures to be as low as $10\times10\,\mu m^2$ or even $6\times6\,\mu m^2$, making whole cell and intracellular measurements feasible (see Chapters 3 and 7). During the course of this project, much progress has also been made in terms of standardization protocols and understanding the contribution of scattering phenomena such as Mie scattering (refer to Chapter 8). In Raman spectroscopy, the diffraction limit applies to the incident monochromatic light source. In the case of FTIR, however, the incident light is not monochromatic, and operating at the diffraction limit can imply reduction of spectral range, as shown in Chapter 2. In terms of spatial resolution, synchrotron IR sources perform significantly better than conventional bench-top instruments due to the

increased beam collimation. Attenuated total reflection imaging techniques have reported spatial resolutions of as low as 2 μm, although this is a significantly more specialized and complex technique.

In terms of axial resolution, for transparent samples, Raman microscopy is governed by the focal depth of the objective, whereas IR microscopy is governed by the thickness of the sample (in simple transmission mode). For a 100× objective, this is typically ~1–2 μm and the axial resolution can be improved by taking advantage of confocal imaging conditions. An important consideration, however, is that whereas in the visible region the majority of cellular components are transparent, many are strongly absorbing in the mid-IR. Thus the nucleus of a cell is optically very dense whereas the cytoplasm is sparse. This has led to many anomalous results indicating that the nucleus is deficient in, for example, nucleic acids compared to the surrounding cytoplasm.[42] The variations in optical density across cells and tissue have led to many confusing results, and effects such as the "dispersion artefact" have entered the vernacular of FTIR spectroscopy. This phenomenon is a direct result of the fact that FTIR is an absorbance technique applied to samples of significant inhomogeneity of optical density and is not manifested in Raman spectroscopy. This stresses the importance of pre-processing FTIR spectra of cells and tissues to avoid such pitfalls and misinterpreting the spectral information, which is not only composed of the sample's biochemical information but also information of physical origins. The physical origin of some of these effects in both transmission and transflection mode have recently been elucidated,[43,44] and a reliable method to remove these artefacts has been proposed (see also Chapter 8).[45]

AQ5

4.8.3 Fluorescence and Scattering

While operating at visible wavelengths in Raman has the advantage of spatial resolution and optical transparency, there are also disadvantages. In general, Raman scattering is inherently a weak process and it suffers from the problem of fluorescence background. If the sample of interest is resonant with the illuminating wavelength, even a low efficiency luminescent emission can be sufficient to swamp the weak Raman signal on the Stokes side. The spectrum of thyroid tissue section in Figure 4.16 was recorded using 514.5 nm irradiation and the background registers in the spectrometer region ~525–630 nm (400 cm^{-1} to 3500 cm^{-1} Raman/Stokes shifted from 514.5 nm) and beyond. This background is commonly assumed to be fluorescence and this assumption has entered the biomedical spectroscopy literature.[46–49] Fluorescence from biomaterials has also been reported at irradiation wavelengths of 785 and even 830 nm.[48,49] It is important to remember, however, that for a material to fluorescence, it must absorb at the irradiating wavelength. Fluorescence spectroscopy has been explored as a potential probe of malignancies in for example skin, the principle chromophores being nicotinamide adenine dinucleotide (NADH), collagen, elastin, tryptophan, flavins and porphyrins.[50] However, excitation wavelengths are typically less than 400 nm and while some chromophores such as

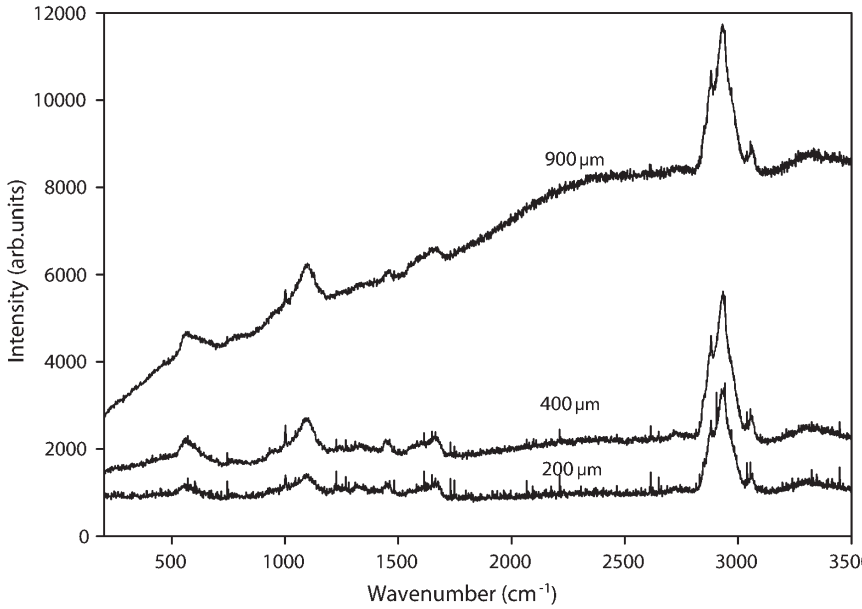

Figure 4.16 Unprocessed Raman spectra of thyroid tissue obtained at an excitation wavelength of 514.5 nm with varying confocal hole.

haemoglobin absorb at visible wavelengths, there is significantly less fluorescence higher than $\sim$600 nm. It must be argued therefore that the large and problematic background to the Raman spectra commonly observed at visible wavelengths may have contributions from a different physical origin.

The background to the Raman spectrum at visible wavelengths can have its origin in stray light from Mie scattering, such that sample morphology can play an important role and the spectral signal to background ratio can be improved by employing a true confocal configuration. Mie scattering occurs upon the interaction of radiation with particles of similar or larger dimensions compared to the incident radiation. Tissue sections have cellular and subcellular features of the order or 1–10 µm. This is in the realm of Mie scattering of visible radiation and gives the sections a white diffuse appearance. It is not surprising therefore that these inhomogeneous samples give rise to a broad background to the Raman spectra. Mie scattering is an elastic process and, since the scattered radiation is of the same frequency as the laser, it should be removed by the holographic notch filter and prevented from entering the spectrometer. The transmission spectrum of the notch filter is however strongly angular dependent. Diffusely scattered radiation is not well collimated by the microscope objective and is thus incident on the notch filter at non-optimized angles. Although it is not well understood, it is assumed that this radiation is transmitted by the notch filter and enters the spectrometer as stray light where, although monochromatic, it appears dispersed across the CCD.

The problems of Mie scattering can be reduced by utilizing the confocality of the microscope configuration. The Mie scattered radiation is not collimated and thus is not transmitted by the confocal hole. Improvements of signal to background of a factor of ~ 10 have been demonstrated in this way (see Figure 4.16).

The measurements reported do not imply that resonant excitation of biological or other materials cannot give rise to fluorescent emission. While the background to the Raman spectra can be viewed as an inconvenience which can be removed either instrumentally or by background removal post spectral recording, fluorescent emission by definition implies a resonant excitation of a chromophore which, when present, through their emission or resonantly enhanced Raman signals could in themselves be valuable as diagnostic or analytical markers. However, as fluorescent efficiencies are in most cases sub unity, any excited state can give rise to local heating and/or photo-oxidative chemistry. With operating powers of 10 mW, this implies a power density of $\sim 10^4\,\mathrm{W\,m^{-2}}$, and while these powers are required given the low efficiency of the Raman effect they can potentially cause significant sample degradation, especially at shorter wavelengths, where the photon energy is high.

4.8.4 Photodegradation

Reports of photodegradation in Raman spectroscopy are indeed numerous. In many cases, however, these are due to multiphoton resonances at high intensities in Optical tweezers or CARS experiments. In a study of photodegradation in Raman spectroscopy of living cells and chromosomes Puppels reported that while significant degradation was observable at 514.5 nm, no degradation was observable at 660 nm [51].[51] It should be noted, however, that even at 514.5 nm, the photon energy (2.4 eV) is not sufficient to cleave a covalent bond. Such a spectral dependence of the photodegradation process is reminiscent of that observed for conjugated organic polymers. In this case the mechanism is one of photo-oxidation whereby a photoexcited species transfers its energy to an oxygen molecule which now in its highly reactive singlet state attacks the donating species causing bond cleavage. In addition to photo-oxidative mechanisms, high power density and absorption can combine to produce thermal damage.[52–54]

It is often necessary to compromise collection efficiency in order to reduce the spotsize and therefore power density while maintaining illumination power to avoid sample degradation. In general in Raman spectroscopy, many intrinsic problems can be avoided by use of near-IR radiation, however. In this way the likelihood of photoexcitation of constituent molecules giving rise to photoemission or photochemistry is reduced. Rayleigh and Mie scattering are similarly reduced. Commonly available near-IR sources supplied with commercial Raman spectrometers are 785 nm and 830 nm laser diodes. On the Stokes shifted side of the Raman spectrum, the "CH" region of the spectrum at 3000–3500 $\mathrm{cm^{-1}}$ is already shifted beyond the sensitivity range of silicon based

CCD systems and therefore 785 nm illumination is accepted as the preferred choice for most biological applications.

4.8.5 Signal to Noise

Ultimately, the Raman effect is intrinsically weak and a limit of the technique is the signal to noise achievable. Raman spectroscopy for the measurement of biochemical changes in tissue depends as much upon the signal to noise (S/N) ratio as the magnitude of the measured Raman signal alone. The S/N ratio is a useful measure describing the quality of the spectrum; its inverse is the relative precision of the measurement, or the relative standard deviation from the true signal. This section aims to quantify the contributions to the Raman spectrum of each common component of noise or source of erroneous signal.

Shot noise is the dominant source of noise in dispersive Raman measurements. It is caused by the random probabalistic nature of light and matter. If the intensity of light is measured with a perfect noise-free detector, the standard deviation of the number of detected photons will be equal to the square root of detected photons.[55] Using an optimized Renishaw System 1000 Raman spectrometer to measure Raman scattering in oesophageal biopsy samples with 830 nm light, the strong C–H stretch band intensity at 1455 cm^{-1} was approximately 4500 counts in 30 s. Therefore the uncertainty of the measurement, due to shot noise, is 67 counts or $\pm 1.5\%$. If the time of acquisition were reduced to 10 s, the measurement would yield 1500 ± 39 counts or $\pm 2.6\%$ uncertainty; a further reduction to an integration time of 1 s would give 150 ± 12 counts or $\pm 8\%$ uncertainty. This example shows the effect of reducing acquisition time leading to a reduction in the S/N ratio and the certainty of the measurement.

It must be noted that the shot noise will not only originate from the Raman scattering signal but also background signal originating from stray light and/or fluorescence. Therefore even if these signals can be subtracted, the shot noise contribution will remain superimposed on the measurement, sometimes completely obscuring the Raman spectrum. For example if the background induced in a sample produces 1000 counts per second at a particular wavenumber of a Raman scattering band that produces 100 counts per second, then the combined signal at the band position will be 1100 counts $\pm$ 33 counts from shot noise. Following subtraction of the background signal of 1000 counts the Raman band has intensity of 100 photons $\pm$ 33 photons or $\pm$ 33% uncertainty. At 830 nm, tissue scattering/fluorescence background has been shown to contribute around 100 counts per second (in this example), whereas the Raman signal can be between 5 and 50 counts per second.

The variation in pixel sensitivity and thermal noise across the CCD detector will superimpose a fixed pattern noise on the Raman spectrum. The effects of these can be reduced by binning several illuminated pixels in the intensity direction; or they can be corrected by collecting a spectrum of light that changes slowly with wavelength and dividing the Raman spectrum by the source

spectrum. (This procedure has been outlined elsewhere.[56]) CCDs have an inherently low dark noise that will depend upon the pixel location, as there will be a temperature gradient from the centre to the edge of the chip, yielding fixed pattern noise plus random noise. CCD detectors are therefore commonly Peltier cooled to $-70\,^{\circ}C$ to minimize thermal noise contributions.

The contribution to the signal in this example from the CCD [Renishaw RenCam (1998)] readout noise was approximately seven electrons per readout. Read noise is a random noise and therefore increases with the square root of the number of readouts per channel. In the case where an active region of 576×20 pixels is used, when reading out 20 pixels separately then the read noise would be around 32 electrons per wavenumber channel (this equates to approximately 6 counts with the Renishaw system in high gain mode). However, if the 20 pixels are binned and digitized together the read noise would be about seven electrons per channel.

Cosmic rays passing through the photosensitive region can produce thousands of photoelectrons. This effect results in a very strong sharp signal in the Raman spectrum. Quantification of spike noise is difficult due to the random nature of its occurrence. However, it is usually quite obvious to the observer when a spectrum of biological tissue contains a contribution from spike noise. These spikes can be erased from the spectrum or the whole spectrum can be discarded. They can also be circumvented by averaging several scans.

The effect of ambient lighting, another source of fixed pattern noise, on tissue Raman spectra should also be considered.

Source noise is caused by fluctuations in the irradiance of the incident light, which inherently causes fluctuations in the Raman scattering. Simultaneous measurement of all spectral components across the CCD array reduces the effect of this noise in an individual spectrum. However, comparison of one spectrum to the next for quantification of biochemical changes is complicated by source noise. The fluctuation in intensity and wavelength of the laser source should also be quantified. This is why the use of stable diode lasers is preferred.

An often neglected source of fixed pattern noise is that caused by instrument alignment and calibration errors. Unwanted information about the performance of the Raman instrument is added to the Raman spectrum. Calibration drift errors should therefore also be considered.

In summary, a typical Raman spectrum of fresh tissue, measured at 830 nm for 30 s with a laser power of 32 mW at the sample, will include a C–H stretch peak at $1445\,cm^{-1}$. If the intensity at this peak is for example 4500 counts then a contribution of 67 counts will be due to shot noise. The total signal of 4500 counts is made up of approximately 3000 counts of fluorescence/stray light signal and 1500 counts of inelastic scattering signal. The contributions from fixed pattern noise sources can be minimized by multiplying the spectra by correction files. Readout noise contributes about 6 counts and the dark current or thermal noise in the CCD contributes approximately 4 counts in the 30 s integration time. Hence measurement repeatability due to quantifiable noise contributions is approximately $\pm5\%$ for the $1445\,cm^{-1}$ peak measured in 30 s.

This can be converted to a quantifiable S/N ratio of 20. The theoretical noise contributions agree well with the measured S/N ratio at 830 nm of 18.5.

4.9 Conclusions

Early detection of disease is critical to successful treatment and reduction of its impacts, *i.e.*, reduced morbidity and mortality. There have been significant advances in Raman technologies that could be exploited for the detection and tracking of molecules, signals or dynamic cellular events in living systems. The challenge is to advance these technologies further to enable the early detection of disease and to monitor disease progression and therapeutic efficacy. Its main advantages lie in the fact that it is chemical-free, offers high spatial resolution and is minimally invasive. It is readily amenable as a novel sensor for diagnostics in whole organisms as well as for miniaturized systems for point-of-care diagnostics. Raman therefore holds promise for bench-top and clinical applications.

Raman analysis holds inherent advantages over FTIR and synchrotron FTIR methodologies. These include higher spatial and spectral resolution and, for biological systems, the weak response of water. Operating at optical or near-IR wavelengths lends further advantages for fibre based *in vivo* applications. Although, in terms of spatial resolution, synchrotron-FTIR is comparable, cost and accessibility is an obvious issue. However, the combination of modalities, *i.e.*, synchrotron-FTIR microscopy with new imaging devices like focal plane arrays (see Chapter 7) or with an ATR imaging should in the future largely improve the potential of IR microscopy in both cell and tissue research.

One of the biggest challenges to moving Raman spectroscopy, as a diagnostic technology, from the laboratory to the health care system is the high computational burden of transforming measurements into some meaningful information that health care providers can use. This also applies to FTIR cell and tissue imaging. Therefore, a very important aspect will be the development of computational techniques and analytical tools for signal extraction/processing and computational modelling of living systems as a predictive tool for therapy, and dealing with large amounts of real-time diagnostic data coming from living systems. The main objective will be to find ways of providing meaningful diagnostic and monitoring information that can be captured efficiently, reliably and in real time (intelligent diagnostic). Such advances will make health care services more efficient, improve patient care and safety, reduce health care costs and/or create opportunities for remote care.

Among the future Raman based techniques, CARS, first reported by Duncan *et al.*,[57] can provide molecular specific contrast,[58,59] with 3D signal localization, due to the fact that multiphoton interactions are required to induce CARS signals in the volume of interest from highly focused, pulsed laser beams.[60] Due to its coherent signal generation it has an advantage over spontaneous Raman scattering microscopy, in that the signals are observed at higher energies relative to the excitation wavelengths. Therefore any fluorescence background from

the sample will not interfere with the signal collected.[60] The most likely applications of this technology will be as a research tool for understanding carcinogenesis processes in *ex vivo* tissue specimens by optically dissecting the sample. It is already capable of rapidly providing high contrast molecular images at the cellular level and should be able to investigate intracellular pharmacokinetics by giving the distribution map of a specific molecule such as a drug.

Surface Enhanced Raman Spectroscopy can provide molecule specific enhancement of Raman signals,[61] by bringing the target molecule into close proximity with a roughened (nanometre scale) noble metal surface. Huge enhancement factors of the order of greater than 10^9 are possible and single molecule detection has been reported.[62] However, it has proved difficult with SERS to achieve reliable and reproducible results, a key requirement for clinical use. Improvements have been made with recent developments of novel substrates such as encapsulated nanoparticles that may overcome some of these difficulties.[63] They can be easily tagged with antibodies and photonic crystals,[64,65] which by careful manufacture can provide reliable substrates that can be tuned to specific resonance with excitation wavelengths. The use of antibody tags to enable molecule specific detection of disease has been demonstrated. Further developments have included the use of SERRS, a resonance SERS technique pioneered by Graham *et al.*, which is able to provide equivalent detection limits to fluorescence labelled dyes.[66] In the cancer environment, tagged nanoparticles enhancing specific signals from malignant markers are either being used *in vivo* (safety issues to be resolved)[67–69] or as molecular specific stains for histopathology;[70–72] with the possibility of numerous multiplexed SERS/SERRS stains providing hyperspectral images of locations of molecules of interest from the same spectral acquisition and tissue section.[73] The application of SERS for intracellular imaging and for monitoring drug distribution at physiological conditions has also been demonstrated.[74]

Uncited Reference

41.

References

1. C. V. Raman and K. S. Krishnan, *Nature*, 1928, **121**, 501.
2. G. Landsberg and L. Mandelstam, *Naturwissenschaften*, 1928, **16**, 557.
3. M. Cardona, X. Zhou and T. Strach, in *Proc. 10th Anniv. HTS Workshop Phys. Mater Appl.*, ed. B. Battlog, World Scientific Singapore, 1996, p. 72–75.
4. C. Adjouri, A. Elliasmine and Y. Le Duff, *Spectroscopy*, 1996, **44**, 46.
5. R. C. Lord and N. T. Yu, *J. Mol. Biol.*, 1970, **20**, 509–24.
6. M. C. Tobin, *Science*, 1998, **161**, 68–69.
7. A. G. Walton, M. J. Deveney and J. L. Koenig, *Calc. Tiss. Int.*, 1970, **6**, 162.

8. N. T. Yu, B. H. Jo, R. C. C. Chang and J. D. Huber, *Arch. Biochem. Biophys*., 1974, **160**, 614.
9. G. J. Puppels and J. Breve, in *''Biomedical Applications of Spectroscopy''*, eds. R.H.J. Clark and R.E. Hester, **vol. 25**, John Wiley and Sons, New York, 1996, Advances in Spectroscopy.
10. M. Gniadecka, H. C. Wulf, O. F. Nielsen, D. H. Christensen and J. Hercogova, *Photochem. Photobiol*., 1997, **66**(4), 418–423.
11. C. M. Krishna, G. D. Sockalingum, L. Venteo, R. A. Bhat, P. Kustagi, M. Pluot and M. Manfait, Evaluation of the suitability of ex-vivo handled ovarian tissues for optical diagnosis by Raman microspectroscopy, *Biopolymers*, **5**, 269–276.
12. J. Smith, C. Kendall, A. Sammon, J. Christie-Brown and N. Stone, *Technol. Cancer Res. Treat*., 2003, **2**(4), 327–331.
13. A. Molckovsky, L.M.W.K. Song, M. G. Shim, N. E. Marcon and B. C. Wilson, *Gastroint. Endosc*., 2003, **57**(3), 396–402.
14. E. B. Hanlon, R. Manoharan, T.-W. Koo, K. E. Shafer, J. T. Motz, M. Fitzmaurice, J. R. Kramer, I. Itzkan, R. R. Dasari and M. S. Feld, *Phys. Med. Biol*., 2000, **45**, R1–R59.
15. P. J. Caspers, G. W. Lucassen, R. Wolthuis, H. A. Bruining and G. J. Puppels, *Biospectroscopy*, 1999, **4**, S31–39.
16. U. Utzinger, A. Mahadevan-Jansen, D. Hinzelman, M. Follen and R. Richards-Kortum, *Appl. Spectrosc*., 2001, **55**(8), 955.
17. N. Stone and P. Matousek, ''Advanced Transmission Raman Spectroscopy – a promising tool for breast disease diagnosis'', *Cancer Res*., 2008, **68**, 4424–4430.
18. N. B. Colthup, L. H. Daly and S. E. Wiberley, *''Introduction to infrared and Raman spectroscopy''*, Academic Press, New York, 1975.
19. E. Smith and G. Dent, *''Modern Raman Spectroscopy: A Practical Approach''*, John Wiley and Sons, New York, 2005.
20. I. R. Lewis and H. G. M. Edwards, *''Handbook of Raman Spectroscopy: From the Research Laboratory to the Process Line''*, CRC Press, 2001.
21. D. A. Long, *''The Raman Effect A Unified Treatment of the Theory of Raman Scattering by Molecules''*, John Wiley and Sons, New York, 2002.
22. F. S. Parker, *''Applications of Infrared, Raman, and Resonance Raman Spectroscopy in Biochemistry''*, Springer-Verlag, Heidelberg, 1983.
23. A. Lewis, J. Spoonhower, R. A. Bogomolni, R. H. Lozier and W. Stoeckenius, *Proc. Natl. Acad. Sci. USA*, 1974, **71**, 4462–4466.
24. R. J. H. Clark and T. J. Dines, *Angewandte Chemie*, 1985, **25**, 131–158.
25. M. Fleischmann, P. J. Hendra and A. J. McQuillan, *Chem. Phys. Lett*., 1974, **26**, 163.
26. D. L. Jeanmaire and R. P. van Duyne, *J. Electroanal. Chem*., 1977, **84**, 1–20.
27. I. Chourpa, F. H. Lei, P. Dubois, M. Manfait and G. D. Sockalingum, *Chem. Soc. Rev*., 2008, **37**(5), 993–1000.
28. S. Nie and S. R. Emory, *Science*, 1997, **275**, 1102.

29. W. M. Tolles, J. W. Nibler, J. R. McDonald and A. B. Harvey, *Appl. Spectrosc.*, 1977, **31**(4), 253–339.
30. G. Eckhardt, D. P. Bortfeld and M. Geller, *Appl. Phys. Lett.*, 1963, **3**, 137.
31. L. D. Ziegler, *J. Raman Spectrosc.*, 2005, **21**, 769–779.
32. E. Ly, O. Piot, A. Durlach, P. Bernard and M. Manfait, *Appl. Spectrosc.*, 2008, **62**, 1088–1094.
33. J. Hutchings, C. Kendall, B. Smith, N. Shepherd, H. Barr and N. Stone, *J. Biophot.*, 2009, **2**, 91–103.
34. F. M. Lyng, E. Ó Faoláin, J. Conroy, A. Meade, P. Knief, B. Duffy, M. Hunter, J. Byrne, P. Kelehan and H. J Byrne, *Exp. Molec. Pathol.*, 2007, **82**, 121–129.
35. T. R. Chowdhury and J. R. Chowdhury, *Acta. Cytol.*, 1981, **25**(5), 557–565.
36. F. Draux, P. Jeannesson, A. Beljebbar, A. Tfayli, N. Fourré, M. Manfait, J. Sulé-Suso and G. D. Sockalingum, *Analyst*, 2009, **134**(3), 542–548.
37. A.D. Meade, C. Clarke, F. Draux, G.D. Sockalingum, M. Manfait, F. M. Lyng, H. J. Byrne. *Anal. Bioanal. Chem.* Jan 20. [Epub ahead of print] (2010).
38. D. A. Moss, M. Keese and R. Pepperkok, *Vib. Spectrosc.*, 2005, **38**(1–2), 185–191.
39. F. Draux, P. Jeannesson, C. Gobinet, J. Sule-Suso, J. Pijanka, C. Sandt, P. Dumas, M. Manfait and G. D. Sockalingum, *Anal. Bioanal. Chem.*, 2009, **395**(7), 2293–301.
40. M. K. Kuimova, K. L. Chan and S. G. Kazarian, *Appl. Spectrosc.*, 2009, **63**(2), 164–71.
41. M. Isabelle, N. Stone, H. Barr, M. Vipond, N. Shepherd and K. Rogers, *Spectroscopy*, 2008, **22**, 97–104.
42. B. Mohlenhoff, M. Romeo, M. Diem and B. R. Wood, *Biophys. J.*, 2005, **88**, 3635–3640.
43. P. Bassan, H. J. Byrne, F. Bonnier, J. Lee, P. Dumas and P. Gardner, *Analyst*, 2009, **134**, 1586–1593.
44. P. Bassan, H. J. Byrne, J. Lee, F. Bonnier, C. Clarke, P. Dumas, E. Gazi, M. D. Brown, N. W. Clarke and P. Gardner, *Analyst*, 2009, **134**, 1171–1175.
45. P. Bassan, A. Kohler, H. Martens, J. Lee, H. J. Byrne, P. Dumas, El. Gazi, M. Brown, N. Clarke and P. Gardner, *Analyst*, 2010, **135**, 268–277.
46. V. Mazet, C. Carteret, D. Brie, J. Idier and B. Humbert, *Chemomet. Intell. Lab. Syst.*, 2005, **76**, 121.
47. C. A. Lieber and A. Mahadevan-Jahnsen, *Appl. Spectrosc.*, 2003, **57**, 1363.
48. J. Zhao, H. Liu, D. I. McLean and H. Zeng, *Appl. Spectrosc.*, 2007, **61**, 1225.
49. E. B. Hanlon, R. Manoharan, T.-W. Koo, K. E. Shafer, J. T. Motz, M. Fitzmaurice, J. R. Kramer, I. Itzkan, R. R. Dasari and M. S. Feld, *Phys. Med. Biol.*, 2000, **45**, R1–R59.
50. R. Na, I.–M. Stender, M. Henriksen and H.- C. Wulf, *J. Invest. Dermatol.*, 2001, **116**, 536.

51. G. J. Puppels, J. H. F. Olminkhof, G. M. J. Segers-Nolten, C. Otto, F. F. M. de Mul and J. Greve, *Exp. Cell Res.*, 1991, **195**, 361.
52. P. P. Calmettes and M. W. Berns, *Proc. Natl. Acad. Sci. USA*, 1983, **80**, 7197–7199.
53. D. O. Lapotko and V. P. Zharov, *Lasers in Surgery and Medicine*, 2005, **36**, 22–30.
54. Y. Liu, D. K. Cheng, G. J. Sonek, M. W. Berns, C. F. Chapman and B. J. Tromberg, *Biophysical Journal*, 1995, **68**, 2137–2144.
55. M. Bass, E.W. Van Stryland, D.R. Williams, W.L. Wolfe Eds, *Handbook of Optics Volume 1, Fundamentals, Techniques and Design*, 2nd edition, McGraw-Hill, New York, 1995.
56. N. Stone, C. Kendall, J. Smith, P. Crow and H. Barr, *Faraday Discuss.: Applications of Spectroscopy to Biomedical Problems*, 2004, **126**, 141–157.
57. M. D. Duncan, J. Reintjes and T. J. Manuccia, *Opt. Lett.*, 1982, **7**, 350.
58. A. Volkmer, *J. Phys. D*, 2005, **38**, R59–R81.
59. J.-X. Cheng and X. S. Xie, *J. Phys. Chem. B.*, 2004, **108**, 827–840.
60. M. ller and A. Zumbusch, *Chem. Phys. Chem.*, 2007, **8**, 2156–2170.
61. M. Fleischmann, P. J. Hendra and A. J. McQuillan, *Chem. Phys. Lett.*, 1974, **26**, 163–6.
62. K. Kniepp, *Phys. Rev. Lett.*, 1997, **78**, 1667.
63. W. E. Doering, M. E. Piotti, M. J. Natan and R. G. Freeman, *Adv. Mater.*, 2007, **19**, 3100–3108.
64. S. Cintra, M. E. Abdelsalam, P. N. Bartlett, J. J. Baumberg, T. A. Kelf, Y. Sugawara and A. E. Russell, *Faraday Discuss.*, 2006, **132**, 191–199.
65. S. Mahajan, M. Abdelsalam, Y. Suguwara, A. Russell, J. Baumberg and P. Bartlett, *Phys. Chem. Chem. Phys.*, 2007, **9**(1), 104–109.
66. G. Sabatte, R. Keir, M. Lawlor, M. Black, D. Graham and W. E. Smith, *Anal. Chem.*, 2008, **80**(7), 2351–2356.
67. A. Pal, N. R. Isola, J. P. Alarie, D. L. Stokes and T. Vo-Dinh, *Faraday Discuss.*, 2006, **132**, 293–301.
68. S. Keren, C. Zavaleta, Z. Cheng, A. de la Zerda, O. Gheysens and S. S. Gambhir, *Proc. Natl. Acad. Sci. USA*, 2008, **105**, 5844–5849.
69. X. M. Qian, X. H. Peng, D. O. Ansari, Q. Yin-Goen, G. Z. Chen, D. M. Shin, L. Yang, A. N. Young, M. D. Wang and S. M. Nie, *Nat. Biotech.*, 2008, **26**, 83–90.
70. L. Sun, K.-B. Sung, C. Dentinger, B. Lutz, L. Nguyen, J. Zhang, H. Qin, M. Yamakawa, M. Cao, Y. Lu, A. J. Chmura, J. Zhu, X. Su, A. A. Berlin, S. Chanand and B. Knudsen, *Nano Lett.*, 2007, **7**, 351–356.
71. B. Lutz, C. Dentinger, L. Sun, L. Nguyen, J. Zhang, A. J. Chmura, A. Allen, S. Chan and B. Knudsen, *Histochem. Cytochem.*, 2008, **56**(4), 371–379.
72. Y. N. Liu, Z. O. Zou, Y. O. Liu, X. X. Xu, G. Yu and C. Z. Zhang, *Spectrosc. Spect. Anal.*, 2007, **27**, 2045–2048.
73. K. Faulds, R. Jarvis, W. E. Smith, D. Graham and R. Goodacre, *Analyst*, 2008, **133**, 1505–1512.
74. I. Chourpa I, F. H. Lei, P. Dubois, M. Manfait and G. D. Sockalingum, *Chem. Soc. Rev.*, 2008, **37**(5), 993–1000.

Addendum A – Raman Calibration Procedure

(a) **Spectral Calibration**

Generally instrument software is based on a linear calibration and thus two reference points are sufficient. In the software, adjustment of the Zero (straight line intercept) and Co-efficient (straight line slope) is possible.

The grating should be tuned to the zero order and the zero point adjusted to ensure agreement. The grating should be tuned to the laser wavelength and the software calibration adjusted accordingly (in cases where the laser line is fixed rather than tuneable, this step is performed upon installation).

The instrument should be focused on a reference sample and the Raman response recorded. Silicon is often recommended as the reference material because it is stable and has a single strong narrow Raman mode at 520.7 cm^{-1} (see Figure 4.2). The Co-efficient parameter should be adjusted to ensure agreement. This can be performed most accurately by fitting a Gaussian/Lorentzian band to the peak.

These steps can be repeated a number of times to ensure a good calibration.

It is recommended at this point also to measure a multiline spectrum from a reference sample (PET, 1,4 Bis (2-methylstyryl) benzene, neon light) so that any nonlinearities of the calibration can be adjusted for in the final data.

(b) **Intensity Calibration**

The intensity calibration can be achieved via the following steps.

Record the dark current response of the detector over the region of interest.

Record the spectrum of a broadband intensity standard. Although white light sources such as halogen or tungsten lamps can be employed, the illumination geometry does not mimic that of the Raman collection well as it does not act as a point source. Thus the use of fluorescent standards (where they exist) such as those provided by the American NIST is recommended, although there are sometimes point to point variations in the signal found from these standards.